This is to certify that the
thesis entitled

FRACTURE PATTERNS OF THE DEVELOPING SKULL
ATTRIBUTABLE TO DIFFERENT IMPACT SCENARIOS

presented by

BRIAN J. POWELL

has been accepted towards fulfillment
of the requirements for the

M.S. degree in Engineering Mechanics

Roger C. Haut
Major Professor's Signature

June 3, 2010
Date

MSU is an Affirmative Action/Equal Opportunity Employer

DATE DUE	DATE DUE	DATE DUE

5/08 K:/Proj/Acc&Pres/CIRC/DateDue.indd

FRACTURE PATTERNS OF THE DEVELOPING SKULL ATTRIBUTABLE TO DIFFERENT IMPACT SCENARIOS

By

Brian J. Powell

A THESIS

Submitted to
Michigan State University
in partial fulfillment of the requirements
for the degree of

MASTER OF SCIENCE

Engineering Mechanics

2010

ABSTRACT

FRACTURE PATTERNS OF THE DEVELOPING SKULL ATTRIBUTABLE TO DIFFERENT IMPACT SCENARIOS

By

Brian J. Powell

Forensic anthropologists and pathologists frequently rely on fracture pattern analysis to determine the causation of trauma in pediatric abuse cases. However, due to a lack of pediatric skull fracture tolerance data it is often difficult to diagnose whether the injury was inflicted or accidental. The research presented in this thesis utilizes an *in situ* porcine head model and finite element analysis to assess the degree and pattern of skull fracture in two different impact scenarios: entrapped and free fall. Chapter 2 documents the skull fracture patterns generated due to a high energy blunt impact using a rigid and compliant interface. The porcine specimens in Chapter 2 were entrapped in a bed of air-hardened epoxy in order to prevent translation of the head during impact. In Chapter 3, the porcine model was used to assess the degree and pattern of fracture due to a free falling head impact. These specimens were dropped with an equal level of impact energy as those in Chapter 2 to compare the patterns of fracture. In Chapter 4, the data from both impact scenarios was compared to assess the differences of fracture. A finite element model was constructed to provide theoretical insight of the principal tensile stress directions for better understanding of the fractures generated in each impact scenario. The information presented in this thesis may be helpful diagnosing whether the head was constrained in a forensic case.

ACKNOWLEDGMENTS

First and foremost, I would like to thank Dr. Roger Haut for his support and guidance in my research and education over the past two years. Also, Dr. Todd Fenton for helping me understand some basic concepts in forensic anthropology. I'd like to thank Cliff Beckett for all of his technical assistance and Ed Reed and Star Lewis for supplying the porcine specimens used for this research. I would like to thank Tim Baumer, M.S. and Nicholas Passalacqua, M.S. for their dedication to the project as a whole. I would like to thank my friends for all the laughs, support and good times through graduate school. Finally, I'd like to thank my family for their unwavering support through the good times and bad. I could not have done it without you!

RESEARCH PUBLICATIONS BY THE AUTHOR

PEER-REVIEWED MANUSCRIPTS

Powell B, Passalacqua N, Baumer T, Fenton T, and Haut R. Fracture Patterns On the Infant Porcine Skull Following Severe Blunt Impact. J. Forensic Sciences. (in review)

Baumer T, Passalacqua N, Powell B, Newberry W, Smith W, Fenton T, and Haut R. Age-Dependent Fracture Characteristics of Rigid and Compliant Surface Impacts on the Infant Skull – A Porcine Model. J. Forensic Sciences. 2009 (in press)

Baumer TG, Powell BJ, Fenton TW, Haut RC, 2009, "Age Dependent Mechanical Properties of the Infant Porcine Parietal Bone and a Correlation to the Human," Journal of Biomechanical Engineering, **131(11)**, pp. 111006-1-6.

PEER-REVIEWED ABSTRACTS

Powell BJ, Passalacqua NV, Baumer TG, Fenton TW, Haut RC. Fracture Patterns on the Infant Porcine Skull Following Severe Blunt Impact. American Society of Mechanical Engineers Summer Bioengineering Conference, Naples, Florida, 2010.

Fenton TW, Passalacqua NV, Baumer TG, Powell BJ, Baumer TG, Newberry WN, Haut RC. A Forensic Pathology Tool to Predict Pediatric Skull Fracture Patterns, Part 2: Fracture quantification and further investigations on infant cranial bone fracture properties. American Academy of Forensic Sciences (AAFS), Seattle, Washington, 2010.

Van Wyhe RC, Powell BJ, Haut RC, Orth MW, Karcher DM. Reducing the growth rate in turkeys improves femoral bone quality. International Poultry Expo, Atlanta, GA, 2010.

Baumer TG, Powell BJ, Fenton TW, Haut RC. Age Dependent Mechanical Properties of the Infant Porcine Skull and a Correlation to the Human. Am. Society of Mechanical Engineering, Lake Tahoe, CA, 2009.

Fenton TW, Passalacqua NV, Baumer TG, Powell BJ, Haut RC. A Forensic Pathology Tool to Predict Pediatric Skull Fracture Patterns - Part 1: Investigations on Infant Cranial Bone Fracture Initiation and Interface Dependent Fracture Patterns. Am. Academy of Forensic Sciences (AAFS), Denver, Colorado, 2009. [*Winner of the Ellis R. Kerley Award*]

TABLE OF CONTENTS

LIST OF TABLES

LIST OF FIGURES

CHAPTER ONE

DEVELOPING THE PORCINE MODEL – AN INTRODUCTION

Head injury is the leading cause of death and permanent disability in children (Tabatabaei and Sedighi, 2008). It is difficult, however, to distinguish inflicted physical abuse from accidental falls due to both scenarios producing similar types of head injuries (Billmire and Myers, 1985). Linear, complex, and depressed skull fractures have been documented in both cases (Reece and Sege, 2000; Wheeler and Shope, 1997). Indeed, skull fracture is diagnosed in 1 of 3 children who are investigated for physical abuse (Belfer et al., 2001). However, non-fatal injury resulting in skull fracture can occur in children less than 12 months of age from a fall from less than 3 feet (Gruskin and Schutzman, 1999). In a study by Belechri et al. (2002), 1,881 cases of falls from bed height reported no fatalities. Attempts have been made in developing a model for pediatric trauma. One such model that has been met with some success scales adult head impact data to predict the impact response of the pediatric head (Prange et al., 2004). However, this model may be unreliable due to the head of a child being much smaller and geometrically different than an adult (Schneider et al., 1986). Also, little information is available on the similarity of skull fracture patterns between adults and children.

Predicting trauma in infants using adult data is also problematic due to the significantly different mechanical properties and structural characteristics of the pediatric skull (Coats and Margulies, 2006). Fetal cranial bone is a very thin, non-homogeneous and highly curved material (McPherson and Kriewall, 1980) while adult bone is a three layered sandwich structure; two cortical bone plates surrounding a porous diploë center (Motherway et al., 2009). In addition, several soft tissue junctions (sutures)

connect skull bones and allow growth of the brain during development. These sutures begin to ossify and interdigitate into adulthood and eventually fuse together, making the skull a single solid structure (Figure 1.1). The posterior and anterior fontanel are also present in the infant skull. These membranous tissues also allow expansion of the brain during development but eventually disappear after the skull bones fuse together. The posterior fontanel is typically closed between birth and eight weeks of age, while the anterior fontanel closes between nine and 26 weeks after birth (Knight, 1991).

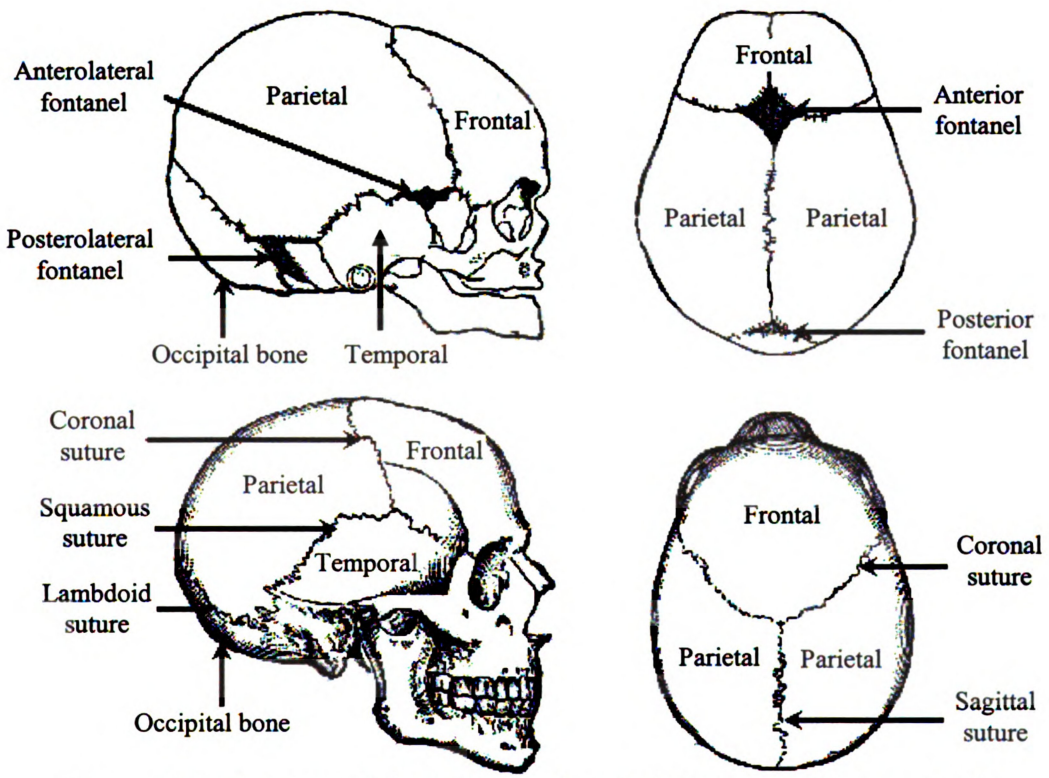

Figure 1.1. Anatomy of the infant (top) and adult (bottom) human skull.

Because of ethical considerations, testing with infant humans is difficult. There is a current lack of studies that utilize infant cadaver specimens to produce data on the impact response of the pediatric head. Infant anthropomorphic surrogates have been used in a recent study (Prange et al., 2003) to document the rotational loading and deceleration conditions of pediatric head impacts. While these studies produce valuable

quantitative data, there are no parts of these surrogates that fail at a given load to simulate bone fracture and the patterns of fracture that are generated during impact (Ewing et al., 1983). Animal models are commonly used for biomechanics studies to generate correlative data to humans. The porcine animal model, in particular, has been used frequently in recent studies. Margulies and Thibault (2000) used porcine skull samples to document age related changes in the mechanical properties of skull bone and suture in three-point bending. Baumer et al. (2009) performed similar studies using four-point bending of porcine skull beam specimens, documenting a skull development relationship of days in pigs to months in infant humans.

In another study, Baumer et al. (In press) impacted the parietal bone on entrapped infant porcine heads using a gravity accelerated mass with rigid and compliant interfaces. The authors document fracture initiation occurring at the bone-suture boundary, remote from the location of impact. Another key finding was that a compliant interface generated more fracture than a rigid interface for a given impact energy. The study, however, was limited to only one, low level of impact energy. It has been thoroughly shown in the literature that the height of a fall (impact energy) has an effect on the degree of injury (Bertocci and Pierce, 2006; Barlow et al., 1983; Wilkins, 1997). A fall from above 1.5 meters increases the severity of injury two fold, and a fall from above 2.5 meters increases the severity of injury three fold (Macarthur et al., 2000; Chalmers et al., 1996). In the process of developing a more robust pediatric fracture model, the effect of impact energy on the length of skull fractures and the pattern of fracture must be examined.

Additionally, the impact scenario must be investigated. Often children sustain head trauma from accidental falls during the development of walking motor skills (Zimmerman and Bilaniuk, 1994). Death from falls is the third leading cause of death in children aged 1-4 years (Hall et al., 1989). In the Baumer et al. (In press) study, the porcine head model was entrapped in a bed of air-hardened epoxy, preventing translation of the head after being impacted with a mass. In a study by Chason et al. (1966), a canine head model that was both fixed and free to move during impact was struck with a rotary mass to assess the effect of head constraint on the degree of concussion. The authors document no skull fracture in the canine specimens, however, they did indicate that there was a higher susceptibility to concussive and neurological problems when the head was fixed during impact. It has been shown in the literature, however, that less force is typically required to produce a concussion than a skull fracture (Rosman, 2004), suggesting that the impact energy levels used by Chason et al. (1966) were not high enough to produce skull fracture. It is therefore unclear what effect constraint of the head has on the degree of skull fracture produced by a blunt impact. Investigation of this issue is also necessary to generate a more robust model of pediatric skull fracture.

In addition to animal models, Finite Element Analysis (FEA) is a powerful and commonly used tool in biomechanics studies. While fracture simulations have extremely high computational costs, it has been noted in the literature that principal stress or strain directions found in finite element simulations correlate well with experimentally and clinically observed fractures (Bozic et al., 1994; Silva et al., 1998). Frank and Lawn (1967) propose that fracture propagates perpendicular to the direction of the greatest principal tensile stress as a method of dissipating the maximum amount of energy in a

system. Thus, it is assumed that the maximum principal stress directions may be used as a predictor of fracture in a finite element simulation.

This thesis presents research conducted on an *in situ* porcine head model, as well as several finite element simulations to assess the effect of impact energy and impact scenario on the degree and pattern of skull fracture. In Chapter 2, fracture length due to a high level of blunt impact energy is documented and compared to previous impacts by Baumer et al. (In press) at lower impact energy levels. Also, the patterns of fracture for the two studies are directly compared in the current study. This study hypothesized that fracture length would be a function of impact energy, specimen age, and impact interface, and that the pattern of fracture would change with a higher level of impact energy. In Chapter 3, a free fall drop tower was built and used to assess the degree of skull fracture and the fracture pattern for a free falling head onto a rigid interface. The free fall fracture patterns were then compared to those in Chapter 2. It was hypothesized that the fracture patterns for these two impact scenarios would be similar. In Chapter 4, the total fracture length, peak impact force, and impact duration data from Chapters 2 and 3 were compared and used in conjuncture with a finite element model to investigate the impact responses of a rigid mass striking a constrained skull and a free falling head onto a rigid surface. The maximum principal stress magnitudes and directions were compared and used to discuss the experimental fracture patterns.

The research conducted for this thesis provides insight into the fracture patterns of the developing porcine skull from two different impact variables: impact energy and impact constraint. A finite element model was also used to validate the experimentally observed differences in the degree of fracturing. These data may ultimately aid in being

able to determine whether the head in a forensic case was constrained or free to move during impact. This information may ultimately prove to be extremely beneficial in helping forensic pathologists and medical examiners to determine whether a trauma was due to accident or abuse.

REFERENCES

Barlow B, Niemirska M, Gandhi RP, Leblanc W, 1983, "Ten years of experience with falls from a height in children," Journal of Pediatric Surgery, **18(4)**, pp. 509-511.

Baumer TG, Passalacqua NV, Powell BJ, Newberry WN, Fenton TW, Haut RC, In Press, "Age-Dependent Fracture Characteristics of Rigid and Compliant Surface Impacts on the Infant Skull – A Porcine Model," Journal of Forensic Science.

Baumer TG, Powell BJ, Fenton TW, Haut RC, 2009, "Age Dependent Mechanical Properties of the Infant Porcine Parietal Bone and a Correlation to the Human," Journal of Biomechanical Engineering, **131(11)**, pp. 111006-1-6.

Belechri M, Petridou E, Trichopoulos D, 2002, "Bunk versus conventional beds: a comparative assessment of fall injury risk," Journal of Epidemiology and Community Health, **56(6)**, pp. 413-417.

Belfer R, Klein B, and Orr L, 2001, "Use of the Skeletal Survey in the Evaluation of Child Maltreatment," American Journal of Emergency Medicine, **19(2)**, pp. 122–4.

Bertocci G and Pierce MC, 2006, "Applications of Biomechanics Aiding in the Diagnosis of Child Abuse," Clinical Pediatric Emergency Medicine, **7(3)**, pp. 194-199.

Billmire ME and Myers PA, 1985, "Serious head injury in infants: accident or abuse?" Pediatrics, **75**, pp. 340-342.

Bozic KJ, Keyak JH, Skinner HB, Bueff UH, Bradford DS, 1994, "Three-Dimensional Finite Element Modeling of a Cervical Vertebra: An Investigation of Burst Fracture Mechanism," Journal of Spinal Disorders & Techniques, **7(2)**, pp. 102-110.

Chalmers DJ, Marshall SW, Langley JD, Evans MJ, Brunton CR, Kelly A, Pickering AF, 1996, "Height and surfacing as risk factors for injury in falls from playground equipment: a case-control study," Injury Prevention, **2(2)**, pp. 98-104.

Chason JL, Fernando OU, Hodgson VR, Thomas LM, Gurdjian ES, 1966, "Experimental Brain Concussion: Morphologic Findings and a New Cytologic Hypothesis," The Journal of Trauma, **6(6)**, pp. 767-779.

Coats B and Margulies SS, 2006, "Material Properties of Human Infant Skull and Suture at High Rates," Journal of Neurotrauma, **23(8)**, pp. 1222-1232.

Ewing CL, Thomas DJ, Sances A, Larson SJ, eds., 1983, "Impact Injury of the Head and Spine," 1st Ed., Springfield, IL: Charles C Thomas.

Frank F and Lawn B, 1967, "On the Theory of Hertzian Fracture," Proceedings of the Royal Society of London, **299(1458)**, pp. 291-306.

Gruskin KD and Schutzman SA, 1999, "Head Trauma in Children Younger Than 2 Years," Archives of Pediatrics and Adolescent Medicine, **153**, pp. 15-20.

Hall JR, Reyes HM, Horvat M, Meller JL, Stein R, 1989, "The Mortality of Childhood Falls," The Journal of Trauma, **29(9)**, pp. 1273-1275.

Knight B, 1991, "Fatal child abuse," In: Forensic Pathology. London: Edward Arnold, pp. 457-73.

Macarthur C, Hu X, Wesson DE, Parkin PC, 2000, "Risk factors for severe injuries associated with falls from playground equipment," Accident Analysis and Prevention, **32(3)**, pp. 377-382.

Margulies SS and Thibault KL, 2000, "Infant Skull and Suture Properties: Measurements and Implications for Mechanisms of Pediatric Brain Injury," Journal of Biomechanical Engineering, **122(4)**, pp. 364-371.

McPherson GK and Kriewall TJ, 1980, "The Elastic Modulus of Fetal Cranial Bone: A First Step Towards An Understanding of the Biomechanics of Fetal Head Molding," Journal of Biomechanics, **13**, pp. 9-16.

Motherway JA, Verschueren P, Van der Perre G, Sloten JV, Gilchrist MD, 2009, "The mechanical properties of cranial bone: The effect of loading rate and cranial sampling position," Journal of Biomechanics, **42**, pp. 2129-2135.

Prange MT, Coats B, Duhaime A, Margulies SS, 2003, "Anthropomorphic simulations of falls, shakes, and inflicted impacts in infants," Journal of Neurosurgery, **99(1)**, pp. 143-150.

Prange MT, Luck JF, Dibb A, Van Ee CA, Nightingale RW, Myers BS, 2004, "Mechanical Properties and Anthropometry of the Human Infant Head," Stapp Car Crash Journal, **48**, pp. 279-99.

Reece RM and Sege R, 2000, "Childhood Head Injuries: Accidental or Inflicted?" Archives of Pediatric and Adolescent Medicine, **154**, pp. 11-15.

Rosman NP, 2004, "Oski's Essential Pediatrics," In: M Crocetti and MA Barone, editors. Oski's Essential Pediatrics. Philadelphia: Lippincott, Williams, and Wilkins.

Schneider L, Lehman R, Pflug M, Owings C, 1986, "Size and Shape of the Head and Neck From Birth to Four Years," Washington, D.C. The Consumer Product Safety Commission, Report No.: UMTRI-86-2.

Silva MJ, Keaveny TM, Hayes WC, 1998, "Computed Tomography-Based Finite Element Analysis Predicts Failure Loads and Fracture Patterns for Vertebral Sections," Journal of Orthopaedic Research, **16(3)**, pp. 300-8.

Tabatabaei SM and Sedighi A, 2008, "Pediatric Head Injury," Iranian Journal of Child Neurology, **2(2)**, pp. 7-13.

Wheeler DS and Shope TR, 1997, "Depressed skull fracture in a 7-month old who fell from bed," Pediatrics, **100**, pp. 1033-1034.

Wilkins, B, 1997, "Head injury – abuse or accident?" Archives of Disease in Childhood, **76(5)**, pp. 393-397.

Zimmerman RA and Bilaniuk LT, 1994, "Pediatric head trauma," Neuroimaging Clinics of North America, **4(2)**, pp. 349-366.

CHAPTER TWO

FRACTURE PATTERNS ON THE INFANT PORCINE SKULL FOLLOWING SEVERE BLUNT IMPACT

ABSTRACT

Traumatic injury to the head accounts for 80% of fatal child abuse cases. However, it is difficult to distinguish abuse from accidental injury is difficult due to similarities in the type of injury. In this chapter, porcine specimens were impacted with a rigid mass at a high level of energy to assess characteristic fracture patterns related to impact interface, specimen age, and level of impact energy. A single impact was delivered to the right parietal bone of 57 specimens aged 2 to 28 days. The impact was generated by releasing a gravity accelerated mass from a controlled height. Paired rigid and compliant impacts of equal energy were conducted for each specimen age. Impact force and contact area were recorded for each impact. Also, skull fracture length was measured to the nearest millimeter. Geographic Information Systems software was used to monitor the frequency of fracture initiation and propagation. Individual maps were generated based on impact interface, specimen age, and impact interface. It was found that impact force increased with age, regardless of interface. Contact area increased with age but was significantly higher in the compliant interface impacts than the rigid. Skull fracture length was greater for the rigid interface than the compliant at all ages except for 2 days. The degree of skull fracture also increased with an increase in impact energy. GIS maps documented additional sites of fracture initiation at a high level of impact energy dependant upon impact interface and level of impact energy. Several unique characteristic fracture patterns were noted as a function of specimen age, impact

interface, and impact energy. These characteristics may prove to be extremely beneficial in establishing the causation of trauma in child abuse cases where the validity of the testimony is questionable or unclear.

INTRODUCTION

Head injuries account for 80% of fatal child abuse in young children (Case et al., 2001). In a study of 89 children under the age of 2 years, 19 of the 20 fatalities were due to abuse (Hobbs, 1984). In contrast, short falls rarely cause serious injury or death in young children (Reiber, 1993). A study of 1,881 falls from bed height reported no deaths (Belechri et al., 2002). Short falls (less than 3 feet), however, can still produce skull fracture in infants less than 12 months of age (Gruskin and Schutzman, 1999). There is currently a lack of data regarding pediatric skull fracture tolerance data and, thus, pediatric trauma with related cranial fracture due to a single-event represents one of the greatest challenges to forensic pathologists and anthropologists.

Distinguishing between accidental and abusive trauma can be difficult, as both may produce similar types of injuries (Billmire and Myers, 1985). Specifically, linear, complex, and depressed skull fractures have been seen in both cases (Reece and Sege, 2000; Wheeler and Shope, 1997). The most commonly fractured cranial bone in accidental and abuse cases is the parietal (Hobbs, 1984; Meservy et al., 1987; Leventhal et al., 1993). The risk of injury is also dependent on the contacting surface (Bertocci et al., 2003). Other variables, such as the area struck, thickness of the skull, thickness of the scalp and hair, and impact direction can also affect the pattern of skull fracture (Knight, 1991; Cooperman and Merten, 2001). To better distinguish pediatric abuse from accident, the aforementioned variables and the magnitude in which they affect skull fracture must be better understood.

A recent study by Baumer et al. (In press) assessed the effects of interface and age using an infant porcine skull impact model, looking specifically at the location of

fracture initiation on the parietal bone. The study shows that impacts from low heights (low energy) typically initiate fractures at a bone-suture boundary. However, in many pediatric death cases there are multiple skull fractures which sometimes extend across suture boundaries (Meservy et al, 1987; Stewart et al., 1993). Multiple, wide or cross-suture fractures are indicative of high energy trauma (Hobbs, 1984). It is therefore necessary to study the effect of high energy impacts as a function of age and interface on the fracture patterns for the pediatric skull.

There were two hypotheses in the current study. First, that the locations of fracture initiation would not depend on the level of impact energy. Rather, it would only depend on age and interface. Secondly, that an increase in impact energy would increase the amount of fracture via propagation for all ages and for both rigid and compliant interfaces. These data will ultimately provide insight into the effect of impact energy on skull fracture patterns due to a single, blunt impact and may provide valuable information that may help distinguish pediatric abuse from accident.

MATERIALS AND METHODS

Porcine specimens were received from a local supplier and stored at -20°C. A total of 57 specimens (aged 2 to 28 days) were used for this study. The animals died of natural causes and were frozen within 12 hours of death. All specimens were free of head injury, which was confirmed during preparation.

The test procedure was described in a previous study (Baumer et al., in press). Briefly, the head was allowed to thaw at room temperature for 24 hours before the scalp and facial tissues on the left side were removed. The specimens were transversely and rotationally constrained in a bed of air-hardened epoxy (Fibre Strand, Martin Senour

Corp., Cleveland, OH). Phosphate-buffered saline (PBS) solution was applied regularly during the preparation. The specimen was placed in a four degree of freedom fixture that allowed adjustments of the impact site (Figure 2.1). The skull was oriented such that the center of the right parietal bone was normal to the impact interface.

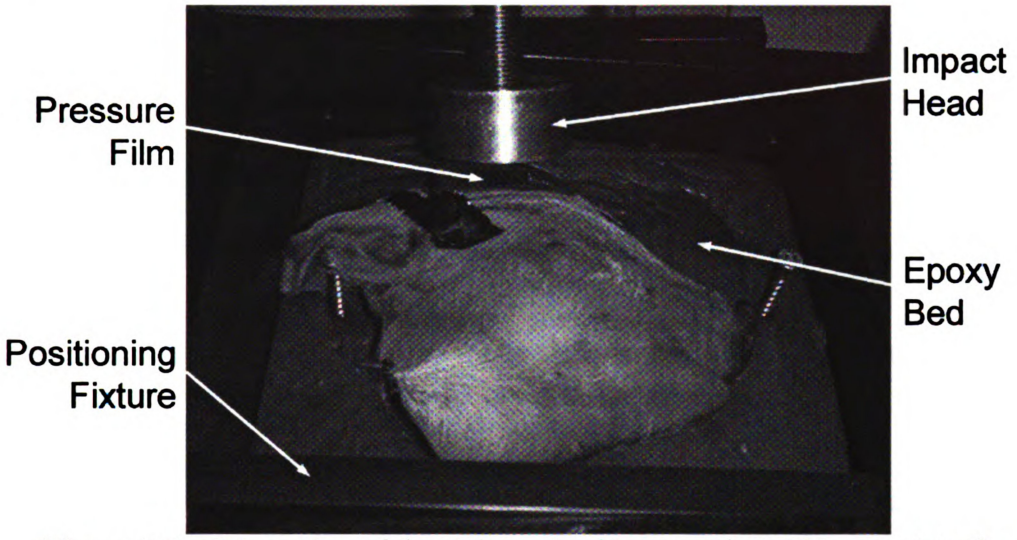

Figure 2.1. Orientation of the right parietal bone with rigid impact interface.

The specimens were impacted using a gravity accelerated mass (GAM) (Figure 2.2). A single impact was delivered using an operational amplifier comparator circuit to monitor the impact force and energize an electromagnetic solenoid to catch the GAM immediately after the impact force returned to zero. The forces were recorded using a load transducer (4.45 kN capacity, model AL311CV, Sensotec, Columbus, OH) mounted immediately behind the impact interface. Two interfaces were used in this study: rigid and compliant. The rigid interface was a solid aluminum cylinder with approximately 16 cm^2 of surface area (Figure 2.1). The compliant interface was a deformable aluminum block (1.10 MPa crush strength Hexcel, Hexcel Corp., Stamford, CT), approximately 3 cm thick with a 16 cm^2 surface area, attached to the rigid interface.

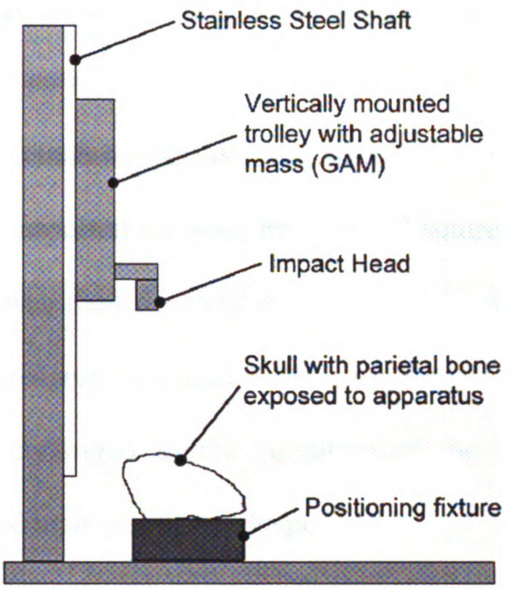

Figure 2.2. The drop tower schematic with GAM shown.

Impact energy was controlled by varying the drop height of a 1.67 kg GAM. A slightly larger, 1.92 kg mass, was used to generate fracture in specimens aged twenty-one days and older. The mass of the impact interface was included in the GAM. Energy levels for each age were double those of a previous study (Baumer et al., in press). The impact energy was doubled by raising the height of the GAM to twice the height of the previous study. The input energy for the compliant and rigid interfaces was equal at each age, however, the impact energy was increased with specimen age. For cases in which the first impact did not cause fracture of the skull (n=5 in the current study), the skull was impacted a second time at a slightly higher energy. The force data was sampled at 10,000 Hz.

Pressure sensitive film packets (Prescale, Fuji Film Ltd., Tokyo, Japan) were attached to the impact site of each specimen to capture contact area. Two sheets of polyethylene were used to protect low (0-10 MPa) and medium (10-50 MPa) range pressure films stacked on top of one other from fluids (Atkinson et al., 1998). The

medium pressure film was not used in the current study as the impact pressures were too low to record on the film.

After impact, the remaining periosteum and soft tissues were removed from the skull and it was visually inspected for bone fracture and suture damage. The remaining soft tissue on the skull was then removed using standard anthropological procedures. The length of skull fractures was measured to the nearest millimeter using a soft, flexible measuring tape, which contoured to the curvature of the skull. Complete fracture diagrams were constructed manually for each specimen.

In order to compare the patterns of fracture between specimens and interfaces, a Geographic Information System (GIS) method was utilized in the study. The pattern of fracture from each skull was constructed using a projected view of the porcine cranium which best highlighted the right side of the skull with fracture configurations superimposed on it for each specimen. A second view of the posterior aspect of the cranium was also included as many high energy fractures involved the occipital bone. Fracture data from Baumer et. al (In press) was also revisited to compare low energy rigid and compliant fracture configurations to the current study. Porcine specimens were separated into two different age groups (2-9 and 19-28 days) for both the rigid and compliant impact interfaces and at low and high energy levels to better demonstrate fracture pattern changes in relation to porcine growth and development, impact interface, and input energy. These age groups were chosen based on general observations of gross fracture and material property changes for the skull and suture tissues documented in the literature (Baumer et al., in press; Baumer et al., 2009). The fracture pattern for each porcine cranium was traced into individual shape files (Marean et al., 2001). The GIS

model then counted overlaid fracture patterns on each cranium, generating a map of where fractures appeared most frequently. After each map was constructed, the GIS model was used to discuss the differences in fracture patterns between specimens of different age, impact energy, and interface.

The impact data were analyzed for age effects using linear regression analyses. Comparisons between the interfaces were performed using a two-factor (age, interface) ANOVA. Statistically significant effects were reported for $p<0.05$.

RESULTS

Impact energies were doubled from those used by Baumer et al. (In press) by doubling the drop height at each age. The drop heights ranged from 0.2 m for a 2 day old specimen to 1.2 m for a 28 day old specimen. The values of impact energy ranged from 3.1 J to 22.6 J, respectively.

The impact force on the skulls increased with age for both interfaces, and there was little difference in the peak impact force (within 100 N at a given age) between the two interfaces (Figure 2.3). Linear regression analysis indicated a significant increase in impact force with age for the compliant ($p<0.001$) and the rigid interfaces ($p=0.006$).

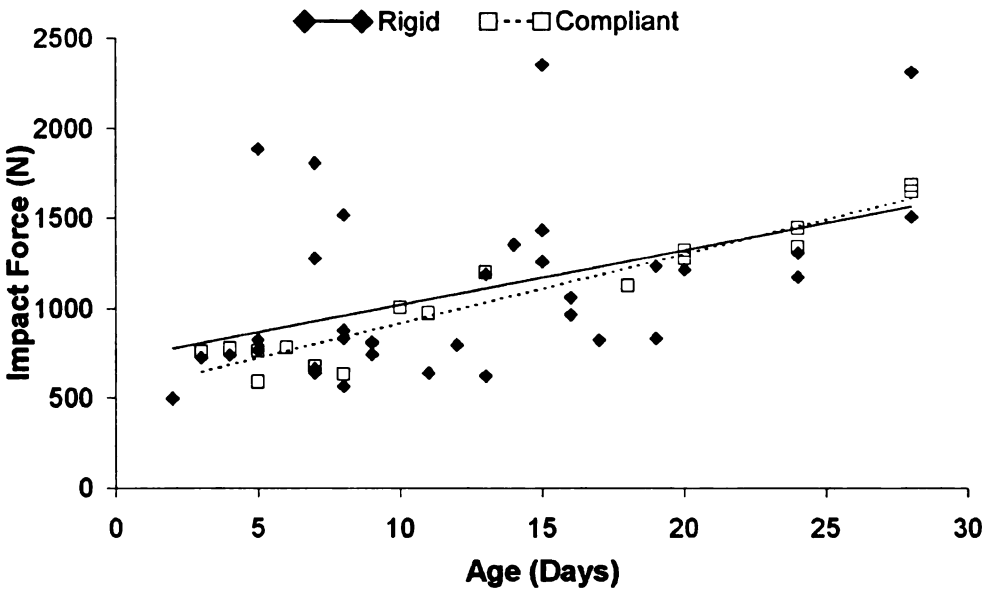

Figure 2.3. Peak impact force versus age for both the rigid and compliant interfaces.

The contact areas generated during impact were found to significantly increase ($p=0.003$) with age at a similar rate for both interfaces (Figure 2.4). A two-factor ANOVA (age, interface) for the contact area showed a significantly larger area of contact generated with the compliant than rigid interface.

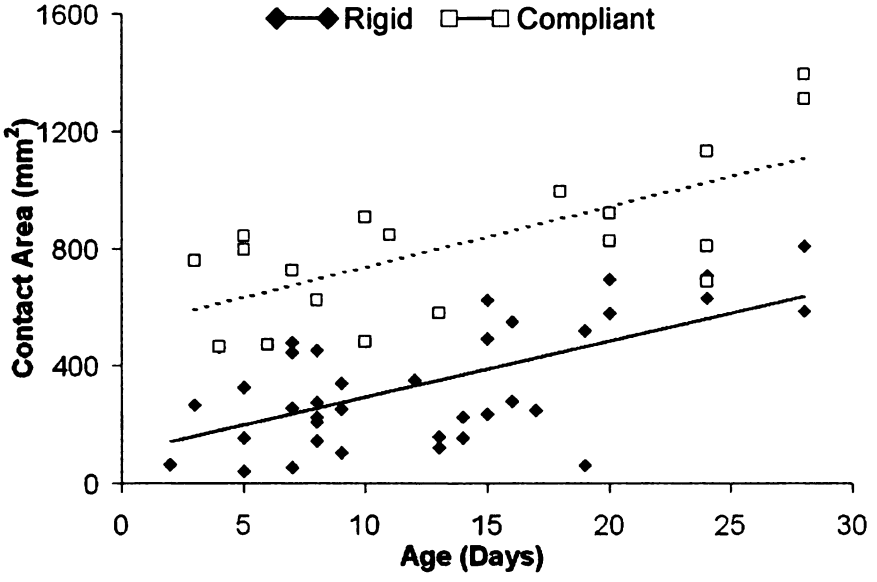

Figure 2.4. Contact area as a function of age for both rigid and compliant interfaces.

The length of fracturing (in bone and along sutures) versus age plot showed, on average, a significantly larger ($p=0.034$) amount of fracturing for the rigid than the compliant interfaces (Figure 2.5).

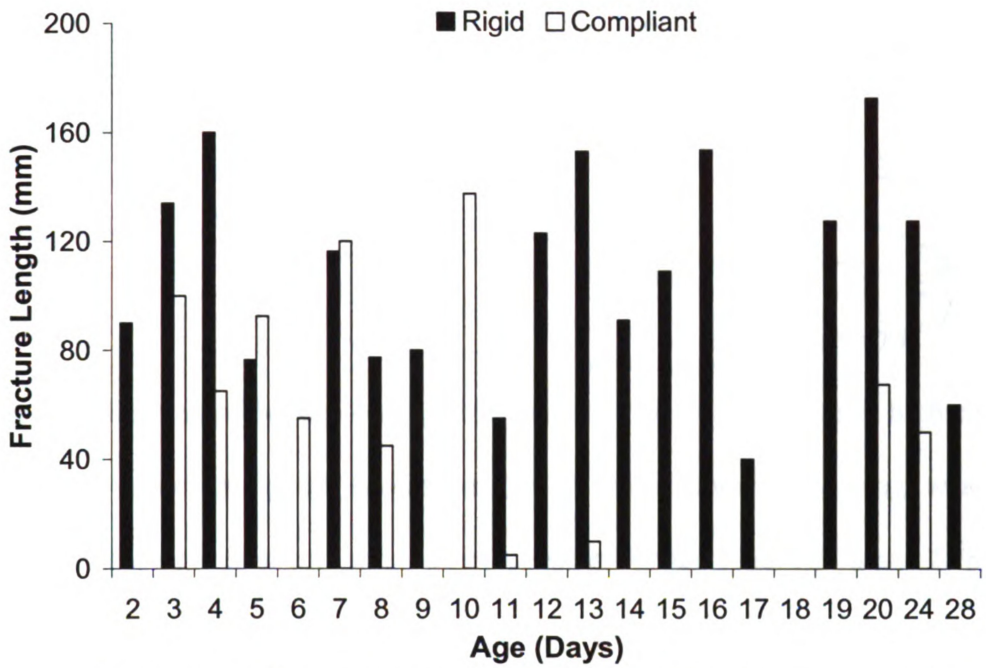

Figure 2.5. The average length of skull fractures as a function of age.

The GIS fracture maps confirmed that the length of fractures was greater for rigid than compliant interface impacts for the younger age group in the current study (Figure 2.6a and 2.6b). For the compliant interface experiments the pattern maps showed fractures primarily appearing to initiate at 4 sites adjacent to sutures along the perimeter of the parietal bone. However, for the rigid, there appeared to be numerous initiation sites. There was also significantly more diastatic fracturing in the rigid than compliant interface experiments, specifically along the coronal suture.

Figure 2.6. GIS map of 2-9 day old rigid (a) and compliant (b) impacts at high energy.

In the older group of specimens (19-28 days) more fracturing was again confirmed for the rigid than compliant interface experiments (Figure 2.7a and 2.7b). Yet, in these experiments, no diastatic fractures were noted. Sites of fracture initiation were evident in the parietal bone along the coronal and lambdoid sutures for the compliant interface experiments. Two of these sites were similar to those documented in the younger age group. These sites were also noted in the rigid interface impacts, however there were more propagated fractures with the rigid interface. Interestingly, in the current study using high energy impacts to the parietal bone, significant fracturing was also documented in the occipital bone for both age groups and interfaces.

Figure 2.7. GIS map of the 19-28 day old rigid (a) and compliant (b) impacts at high energy.

The GIS maps of the revisited Baumer et al. (In press) data showed three primary areas of fracture initiation, regardless of interface. For the younger age group (2-9 days old), the compliant interface produced more fracture of the skull than the rigid at the same impact energy level (Figure 2.8a and 2.8b).

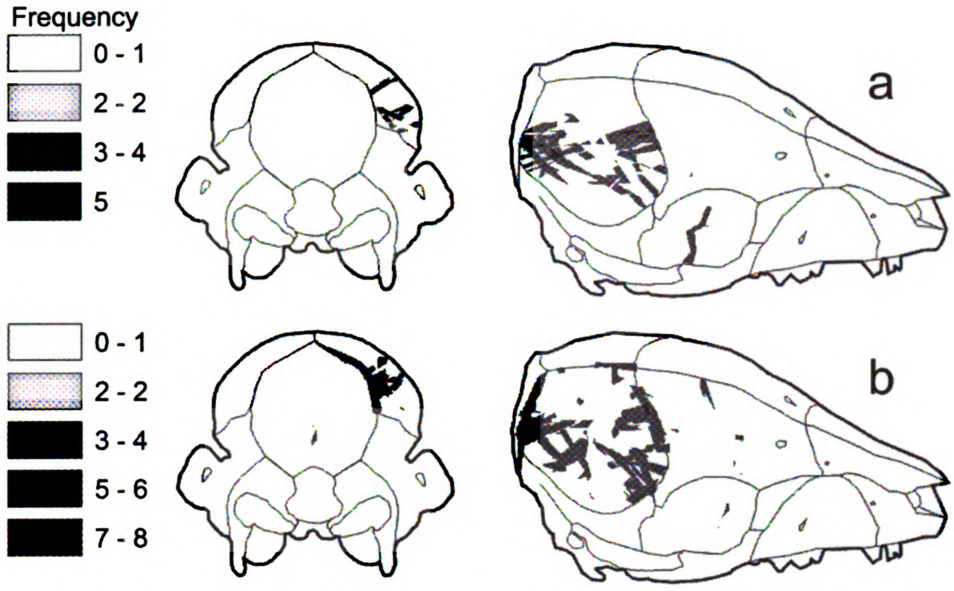

Figure 2.8. GIS map of the 2-9 day old rigid (a) and compliant (b) impacts at low energy.

For a low energy of impact there was little to no skull fracture with the compliant interface for the older age group (Figure 2.9b). Two fracture initiation sites were noted along the coronal and lambdoid sutures. The rigid impacts produced more propagated fractures initiating at approximately the same locations as in the compliant interface experiments (Figure 2.9a).

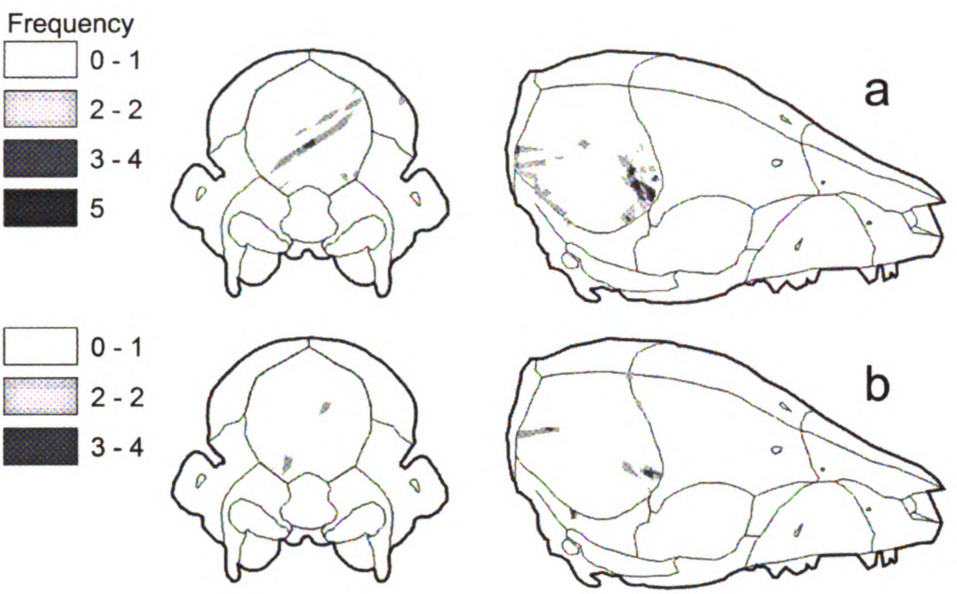

Figure 2.9. GIS map of the 19-28 day old rigid (a) and compliant (b) impacts at low energy.

There were many specimens in both high energy age groups where fractures appeared in the occipital region. These fractures were not present in the revisited Baumer et al. (In press) data.

DISCUSSION

The current study focused on skull fracture patterns under a high impact energy as a function of both age and interface using a porcine model. It was hypothesized that a high level of impact energy would not change the locations of fracture initiation from those documented previously in low energy experiments (Baumer et al., in press). However, the locations of fracture initiation were found to be a function of impact energy. Baumer et al. (In press) document three primary sites of fracture initiation for both interfaces at a low impact energy. While these sites were present in the current study, new initiation sites emerged at the increased level of impact energy. It was also hypothesized in the current study that there would be a greater amount of fracturing via

propagation for these higher energy impacts. The amount of fracture produced in the current study was significantly greater than that produced in the low energy experiments conducted by Baumer et al. (In press).

An interesting finding in the Baumer et al. (In press) study was the equal amount of fracture produced by the rigid and compliant interfaces at approximately 18 days of age for a given impact energy. Prior to 18 days, the compliant interface produced more fracture than the rigid interface, but thereafter there was less for the same impact energy. Baumer et al. (In press) suggest that the compliant interface generated higher states of stress near sutures. These stresses were high enough to produce diastatic fractures and therefore a larger amount of total fracture with the compliant interface. In the current study, however, the rigid interface produced more fracture than the compliant interface at all ages, except for the 2 day old specimens. This change may be attributable to alterations in bone and suture sensitivities to rate of loading. It has been shown in the literature that human bone and suture exhibit mechanical property sensitivities to loading rate (Wood, 1971; Yoganandan et al., 1995; Motherway et al., 2009). Young soft tissues, in particular, are more sensitive to changes in loading rate than older tissues (Haut, 1983). Margulies and Thibault (2000) also determined the material properties of young porcine cranial suture at two different rates of loading and document significant increases in rupture modulus, elastic modulus and rupture energy at the higher rate. Therefore, at higher rates of loading, sutures may become more "brittle-like", especially in the younger aged specimens. The rigid interface may have produced more fracture due its smaller contact area, which produced higher impact stresses than the compliant interface. Furthermore, with an increase in suture stiffness for these high rates of loading

in the current study higher stresses were likely transmitted across sutures to produce fracture in the occipital bone with both interfaces. These results contrast with the lack of occipital fracture documented in the Baumer et al. (In press) study at low levels of impact energy. These findings suggest that high levels of impact energy generate more areas of fracture remote to the impact site.

The greater degree of total skull fracture in the current study was also due to new sites of fracture initiation with increased levels of impact energy. Baumer et al. (In press) document three primary sites of fracture initiation, regardless of interface (Figure 2.8a and 2.8b) at low energy. These three sites were also documented in the current study, however, there were one or more additional sites of fracture initiation depending on interface. One possible explanation for these new sites is the need to dissipate a larger amount of energy through fracture of the bone. In the current study, the initiation sites documented by Baumer et al. (In press) were fully propagated through the parietal bone for the rigid interface. Fracture propagation appeared to be one method to dissipate impact energy, however, additional fractures sites were likely needed to allow the bone to dissipate all of the impact energy generated with the higher drop heights in the current study. These new sites were more frequent with the rigid interface due to the impact force being distributed over a smaller area, generating larger impact stresses in the skull. The larger contact area produced with the compliant interface likely attenuated impact stresses resulting in fewer fracture initiation sites. This difference in fracture initiation sites suggests that the level of impact energy affected a characteristic feature of the fracture pattern for a given interface.

The commonality in fracture patterns for the current and Baumer et al. (In press) studies between specimens of the same age and impacted with the same interface was documented using GIS software. This GIS image-analysis approach has been previously used for both archaeological cut-mark distribution on fauna (Abe et al., 2002) and carnivore modification to faunal remains (Hodgson et al., 2009), however, while Damann et al. (2009) have examined fracture patterns from human aircraft crashes, this is the first forensic application of the Marean et al. (2001) GIS image-analysis technique for bone fracture pattern analysis. Further, this project is unique as it is one of the first attempts to compile fracture pattern data from a relatively large sample of documented experimental impacts. Lee (1992) examined fracture patterns of human laryngeal structures after impacting them with a drop-tower, but this analysis did not employ GIS, instead using simple tracings of fracture lines. The analyses in the current study provided some insight into the discrimination of fracture characteristics as a function of specimen age, impact interface and energy. These characteristics were described by assessing the frequency of fracture on each GIS map for a given set of impact conditions. For example, high energy impacts in the younger age group (2-9 days) tended to produce occipital fracture for both interfaces. Again, occipital fracture was not seen in the low energy impacts. Additionally, each interface produced characteristic fracture attributes. The rigid interface generated much diastatic fracturing at the higher impact energy, whereas the compliant interface did not. These findings contrast with those noted by Baumer et al. (In press) where the compliant interface produced more diastatic fractures than the rigid interface for the younger aged specimens. One could then say, if a given fracture pattern for a younger aged victim involves occipital and diastatic fracture, the

causation of injury could have been due to a high energy, rigid impact. Future work should focus on the study of uniqueness of the characteristic features of fracture patterns on the infant porcine skull as a function of impact interface, energy, and specimen age. While there are certain age limitations of the porcine model (after approximately 24 days the skull geometry begins to differ significantly from humans), it could be used as an experimental model to help develop a better understanding of these characteristics.

In cases of suspected child abuse, the medical examiner faces a difficult task in determining the causation of trauma. Age, interface and impact energy each appear to affect the pattern and degree of skull fracture. In the current study, rigid and compliant interfaces were compared at a given specimen age under a high impact energy. The rigid interface produced as much or more fracture as the compliant at each age. This was in contrast to previously reported data for low energy level impacts where a compliant interface produced more fracture of the infant porcine skull for specimens less than 18 days of age (Baumer et al., in press), and less for more aged specimens. The current study also showed that a higher versus lower levels of impact energy in previous studies altered the pattern of skull fracture by generating new sites of fracture initiation and causing fracture in adjacent bones of the skull. Some unique characteristics of these fracture patterns as a function of energy and interface were also assessed in the study using GIS software. Development of these characteristics may prove to be extremely beneficial in the task of investigating cases of potential abuse to infants.

REFERENCES

Abe Y, Marean CW, Nilssen PJ, Assefa Z, Stone EC, 2002, "The analysis of cutmarks on archaeofauna: A review and critique of quantification procedures, and a new image-analysis GIS approach," American Antiquity, **67(4)**, pp. 643-663.

Atkinson PJ, Newberry WN, Atkinson TS, Haut RC, 1998, "A method to increase the sensitive range of pressure sensitive film," Journal of Biomechanics, **31(9)**, pp. 855-859.

Baumer TG, Passalacqua NV, Powell BJ, Newberry WN, Fenton TW, Haut RC, in press, "Age-Dependent Fracture Characteristics of Rigid and Compliant Surface Impacts on the Infant Skull – A Porcine Model," Journal of Forensic Science.

Baumer TG, Powell BJ, Fenton TW, Haut RC, 2009, "Age Dependent Mechanical Properties of the Infant Porcine Parietal Bone and a Correlation to the Human," Journal of Biomechanical Engineering, **131(11)**, pp. 1-6.

Belechri M, Petridou E, Trichopoulos D, 2002, "Bunk versus conventional beds: a comparative assessment of fall injury risk," Journal of Epidemiology and Community Health, **56**, pp. 413-417.

Bertocci GE, Pierce MC, Deemer E, Aguel F, Janosky JE, Vogeley E, 2003, "Using Test Dummy Experiments to Investigate Pediatric Injury Risk in Simulated Short-Distance Falls," Archives of Pediatrics and Adolescent Medicine, **157(5)**, pp. 480-486.

Billmire ME and Myers PA, 1985, "Serious head injury in infants: accident or abuse?" Pediatrics, **75**, pp. 340-342.

Case ME, Graham MA, Handy TC, Jentzen JM, Monteleone JA, 2001, "Position Paper on Fatal Abusive Head Injuries in Infants and Young Children," The American Journal of Forensic Medicine and Pathology, **22**, pp. 112-122.

Cooperman DR and Merten DF, 2001, "Skeletal Manifestation of Child Abuse," In: RM Reece & S Ludwig, editors. Child Abuse: Medical Diagnosis and Management. Philadelphia: Lippincott, Williams, and Wilkins.

Damann FE, Adler R, Benedix DC, Kontanis EJ, 2009, "Patterns of perimortem fracture from military aircraft crashes," Proceedings of the American Academy of Forensic Sciences; Washington D.C.

Gruskin KD and Schutzman SA, 1999, "Head Trauma in Children Younger Than 2 Years," Archives of Pediatrics and Adolescent Medicine, **153**, pp. 15-20.

Haut RC, 1983, "Age-Dependent Influence of Strain Rate on the Tensile Failure of Rat-Tail Tendon," Journal of Biomechanical Engineering, **105(3)**, pp. 296-299.

Hobbs CJ, 1984, "Skull Fracture and the Diagnosis of Abuse", Archives of Disease in Childhood, **59**, pp. 246-252.

Hodgson JA, Plummer TW, Forrest F, Bose R, Oliver JS, 2009, "A GIS-based approach to documenting large canid damage to bones," Proceedings of the 78th annual meeting of the American Association of Physical Anthropologists; Chicago, IL.

Knight B, 1991, "Fatal child abuse," In: Forensic Pathology. London: Edward Arnold, pp. 457-73.

Lee SY, 1992, "Experimental blunt injury to the larynx," The Annals of Otology, Rhinology, and Laryngology, **101(3)**, pp. 270-274.

Leventhal JM, Thomas SA, Rosenfield NS, Markowitz RI, 1993, "Fractures in young children: distinguishing child abuse from unintentional injuries," American Journal of Diseases of Children, **147**, pp. 87-92.

Marean CW, Abe Y, Nilssen PJ, Stone EC, 2001, "Estimating the Minimum Number of Skeletal Elements (MNE) in Zooarchaeology: A Review and a New Image-Analysis GIS Approach," American Antiquity, **66(2)**, pp. 333-348.

Margulies SS and Thibault KL, 2000, "Infant Skull and Suture Properties: Measurements and Implications for Mechanisms of Pediatric Brain Injury," Journal of Biomechanical Engineering, **122(4)**, pp. 364-371.

Meservy CJ, Towbin R, McLaurin RL, Myers PA, Ball W, 1987, "Radiographic characteristics of skull fractures resulting from child abuse," American Journal of Roentgenology, **149**, pp. 173-175.

Motherway JA, Verschueren P, Van der Perre G, Sloten JV, Gilchrist MD, 2009, "The mechanical properties of cranial bone: The effect of loading rate and cranial sampling position," Journal of Biomechanics, **42(13)**, pp. 2129-2135.

Reece RM and Sege R, 2000, "Childhood Head Injuries: Accidental or Inflicted?" Archives of Pediatric and Adolescent Medicine, **154**, pp. 11-15.

Reiber GD, 1993, "Fatal falls in childhood: How Far Much Children Fall to Sustain Fatal Head Injury?" American Journal of Forensic Medicine and Pathology, **14**, pp. 201-207.

Stewart G, Meert K, Rosenberg N, 1993, "Trauma in infants less than three months of age," Pediatric Emergency Care, **9(4)**, pp. 199-201.

Wheeler DS and Shope TR, 1997, "Depressed skull fracture in a 7-month old who fell from bed," Pediatrics, **100**, pp. 1033-1034.

Wood J, 1971, "Dynamic Response of Human Cranial Bone," Journal of Biomechanics, **4(1)**, pp. 1-12.

Yoganandan N, Pintar FA, Sances A, Walsh PR, Ewing CL, Thomas DJ, et al., 1995, "Biomechanics of Skull Fracture," Journal of Neurotrauma, **12(4)**, pp. 659-669.

CHAPTER THREE

FRACTURE LENGTH AND PATTERN OF THE PORCINE HEAD MODEL IN FREE FALL

ABSTRACT

Head trauma is the leading cause of death in infants. Often, children sustain head trauma during normal activities and play which are deemed accidental and innocent. In the previous chapter, the degree and pattern of skull fracture was investigated after a porcine head model, entrapped in a bed of air-hardening epoxy, was struck with a blunt mass. This scenario, however, does not reflect the common injury occurrence from accidental falls. In the current study the porcine head model was dropped in free fall to assess the pattern of fracture generated from an unconstrained fall from a controlled height. A mounting plate and clamp was used to orient the right parietal bone normal to the rigid impact interface. A drop trolley translating along a vertical stainless steel shaft attached to a drop tower provided motion in only the vertical direction. Drop heights were calculated from previously used impact energy values in Chapter 2 in order to produce an equal amount of free fall impact energy to the skull. The Geographic Information Systems method was again used to map the frequency of fractures in the parietal, frontal and occipital bones. Total fracture length steadily decreased with age in the free fall head impacts. The results also showed that the pattern of fracture differed significantly between the free fall impacts and entrapped impacts regardless of age. The extensive levels of occipital bone fracture documented in Chapter 2 was not seen in the free fall impacts, even though the same impact energy was used. Additionally, there were significantly fewer sites of fracture initiation in the free fall impacts than in the

entrapped impacts. These sites were age dependent with younger specimens having fracture initiation along the coronal suture and older specimens having fracture initiation sites on both the posterior and anterior edges of the parietal bone along the coronal and lamdoid sutures. Diastatic fracture was documented in both age groups but not in specimens older than 14 days of age. The patterns of fracture presented here are significantly different and are representative of two cases of equal high level of energy head impacts. One case is a fall with a given energy onto a rigid surface and the second case is a head that is on a rigid surface being struck with a blunt object. The research presented in this chapter may be extremely beneficial to medical examiners and forensic pathologists in determining the cause of skull fracture in cases of potential pediatric abuse.

INTRODUCTION

Traumatic injury to the head is the leading cause of death in infant humans (Tabatabaei and Sedighi, 2008). Often children sustain head trauma due to accidental falls during the development of walking motor skills or from child support devices such as highchairs (Zimmerman and Bilaniuk, 1994; Mayr et al., 1999). Pediatric falls typically result in impacts to the head due to the increased weight ratio of the head to the body as compared to adults (Yoganandan and Pintar, 2004; Snyder, 1977; Smith et al., 1975; Cory et al., 2001). Death resulting from falls is the third leading cause of death in infants aged 1-4 years of age (Hall et al., 1989). However, in a study of 89 children under 2 years of age, 19 of the 20 fatalities were attributed to physical abuse (Hobbs, 1984). Linear, complex, and depressed fractures have been documented in both abuse and accidental cases (Reece and Sege, 2000; Wheeler and Shope, 1997). Thus, distinguishing an accident from inflicted abuse is difficult due to both scenarios producing similar types of injury (Billmire and Myers, 1985). Due to a lack of pediatric cranial trauma data, correctly diagnosing skull fracture due to abuse or from an accidental fall poses a significant challenge to medical examiners and forensic pathologists and anthropologists.

Injury biomechanics are used in case-based investigations of suspected child abuse (Bertocci and Pierce, 2006). Animal models are often used in these cases to correlate data to humans. A porcine head model has been recently used in this laboratory to assess the effect of a blunt impact to the parietal bone of the skull. Baumer et al. (In press) document fracture initiation sites occurring at the bone-suture boundary, remote of the point of impact. Similarly, in Chapter 2, skull fracture patterns were assessed to

distinguish unique characteristics due to impact interface, age of specimen, and impact energy. In both studies, the porcine head was entrapped in a bed of epoxy and impacted with a rigid mass. Chason et al. (1966) impacted a canine head model that was both fixed and free using a rotary striker. Interestingly, the authors documented that there was a higher susceptibility to concussion when the head was fixed rather than free to move. The authors also documented a lack of skull fracture in all of the specimens. It has been shown, however, that there is typically less force required to produce a concussion than a skull fracture (Rosman, 2004) and thus the energy levels used in the Chason et al. (1966) study may not have been high enough to produce skull fracture. Thus, it is unclear what effect constraint of the head during impact has on the degree and pattern of skull fracture. Therefore, in the current study, the porcine head model was dropped in free fall to assess the degree of skull fracture length as well as the fracture pattern.

The hypothesis of this study was that the pattern of fracture in the free fall impact would be similar to those found in the entrapped impacts from Chapter 2 for an equal impact energy. These data may ultimately provide utility for forensic pathologists and anthropologists in comparing fracture data from potential pediatric abuse cases to known impact conditions using the porcine head model. If there are differences in fracture pattern between a constrained head impact versus a free fall head drop, it may be possible to determine if the victim's head was constrained or free to move during the impact.

MATERIALS AND METHODS

A total of 31 porcine specimens were received from a local supplier and stored at a temperature of -20°C. All animals had died of natural causes and were frozen within

12 hours of death. The specimens ranged from 2-17 days of age. Each animal was inspected for initial head injury by palpating the parietal bone prior to experimentation.

Each specimen was fastened to a mounting plate using Velcro straps. A four degree of freedom clamp directly attached to the mounting plate was used to orient the parietal bone normal to the impact interface. The mounting plate was fastened to a hollow aluminum rod which was supported by a gravity accelerated drop trolley. The rod was clamped with an electromagnetic solenoid, acting as a catch and release mechanism, attached to the drop trolley. The drop trolley was constricted to linear translation in the vertical direction by a stainless steel shaft attached to a drop tower chassis (Figure 3.1). To produce the necessary impact energy, the drop trolley was raised to the necessary drop height and held in place by a second electromagnetic solenoid. The solenoid was fastened to a crossbar to adjust the drop height to a maximum of 9 feet. During the experiment, both solenoids disengaged, allowing the drop trolley and mounting rod to fall freely (Figure 3.2).

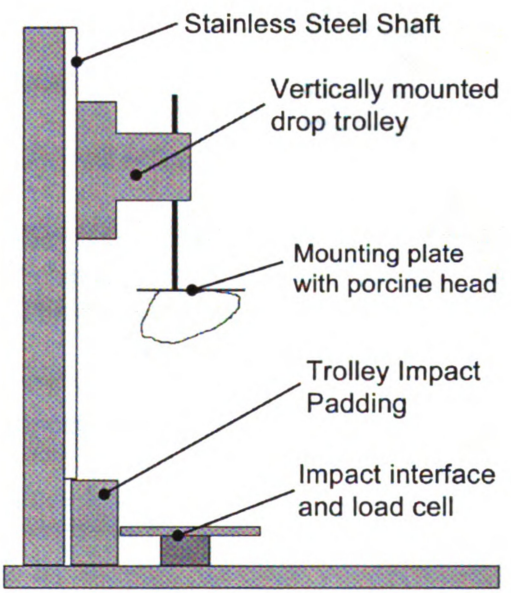

Figure 3.1. Schematic of the free fall drop tower.

Upon impact, the trolley base struck a soft padded surface to dissipate the drop energy in the trolley. The skull impacted a rigid, aluminum interface with an approximate surface area of 324 cm^2. A load cell (2.22 kN capacity, model 1010AF-500, Interface, Scottsdale, AZ) mounted immediately behind the impact interface recorded impact force, duration, and energy. The skull was allowed to impact only once by using an operational amplifier comparator circuit to monitor the impact and reenergize the electromagnetic solenoid to catch the rod immediately after the impact force returned to zero. The force data were sampled at 10,000 Hz.

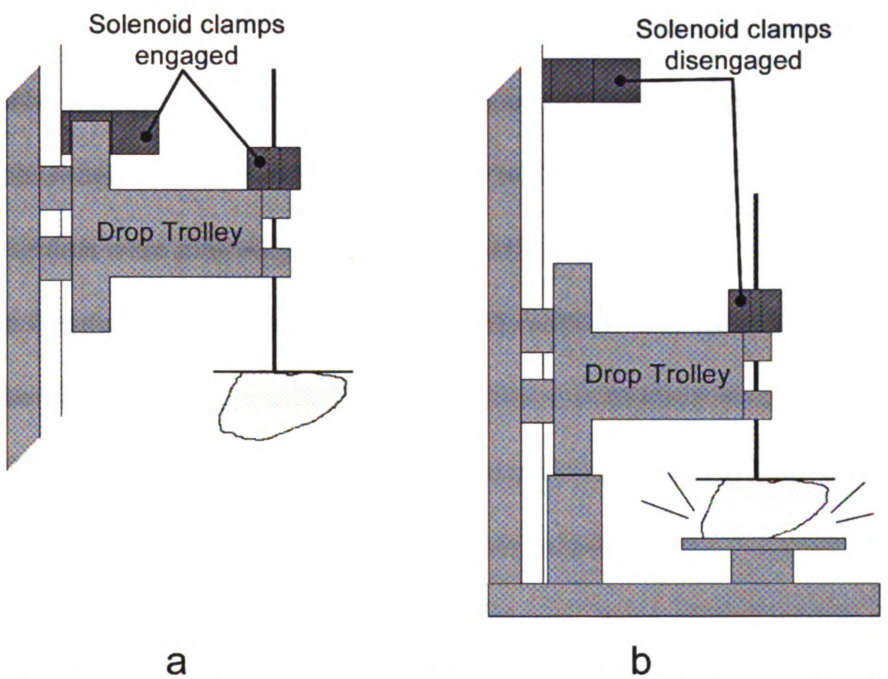

Figure 3.2. The drop trolley was raised to the necessary drop height and held with the electromagnetic solenoid clamp (a). The free fall impact was produced by disengaging the solenoid clamps (b). The mounting rod was free to move vertically until the impact force returned to zero.

In Chapter 2, entrapped porcine specimens were impacted using a high level of impact energy. Energy values for each age of specimen were matched in this chapter to those used in Chapter 2 by varying the drop height of each specimen. Due to the

differences in mass of the head with age, each specimen's head mass was measured and given a respective drop height to match the Chapter 2 impact energies at each age using

$$U = m * g * h \tag{4.1}$$

where U was the potential impact energy, m was the mass of the head, g was the gravitational acceleration, and h was the respective drop height.

Each skull was dropped only once regardless if skull fracture was present. After impact, the scalp and soft tissues of the skull were removed using standard anthropological procedures. Each skull was visually inspected for fractures and photo documentation was taken. The periosteum and remaining soft tissues were then removed. The length of skull fracture was measured to the nearest millimeter using a soft, flexible measuring tape, which contoured to the curvature of the skull. Complete fracture diagrams were manually constructed for each specimen.

The Geographic Information System (GIS) method was again used in this chapter to map the frequency of fractures. The pattern of fracture from each skull was constructed using a projected view of the porcine cranium which best highlighted the right side of the skull with superimposed fracture configurations for each specimen. A second view of the posterior aspect of the cranium was also included to display fractures of the occipital bone. The porcine specimens were again separated into two different age groups (2-9 and 10-17 days) to demonstrate fracture pattern changes in relation to porcine growth and development, as well as the impact scenario. Fracture pattern data from Chapter 2 were revisited to compare the fracture patterns of the 2-9 day old and 10-17 day old age groups from high energy, rigid interface, entrapped impacts to the free fall experiments. The age groups were chosen based on the available specimens, as well

as general observations of gross fracture and material property changes for the skull and suture tissues documented in the literature (Baumer et al., in press; Baumer et al., 2009). The pattern of fracture for each porcine cranium was traced into individual shape files (Marean et al., 2001). The GIS software then counted overlaid fracture patterns on each cranium, generating a map of where fractures appeared most frequently. After each map was constructed, the GIS maps were used to compare the patterns of fracture produced from free falls and entrapped impacts using the same energy.

Impact force and total fracture length were analyzed for age effects using linear regression analyses in a statistics software (SigmaStat 2.03, Aspire Software International, Ashburn, VA). Statistically significant effects were reported for a p-value of less than 0.05.

RESULTS

The aim of the current study was to assess the impact characteristics of a porcine head dropped in a free fall scenario. There was a characteristic rapid drop in force documented in the force-time plots, which was associated with skull fracture (Figure 3.3). A more pronounced peak was noted if no fracture was present.

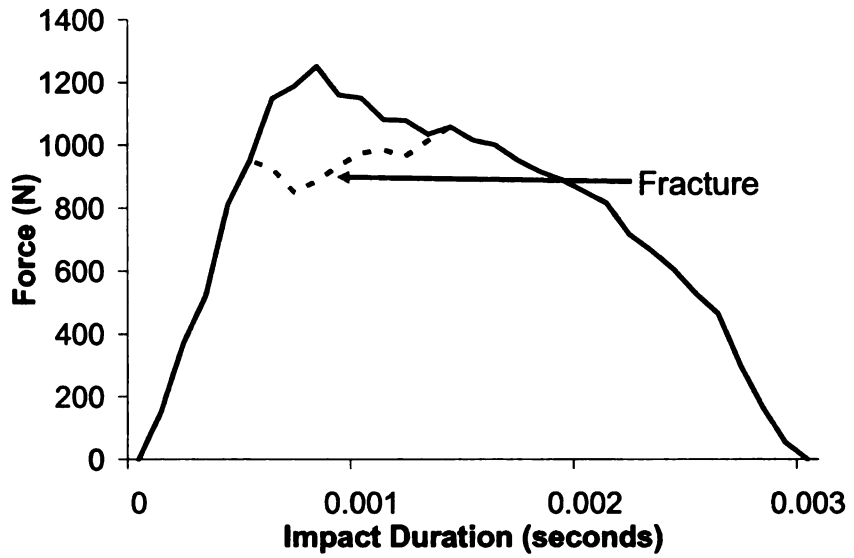

Figure 3.3. An overlay of force-time plots showing the characteristic rapid drop in force associated with skull fracture.

Peak impact force significantly increased with age at a rate of 40.9 N/day of age ($p<0.001$) (Figure 3.4). Also, impact energy significantly increased with age at a rate of 0.19 J/day ($p=0.009$).

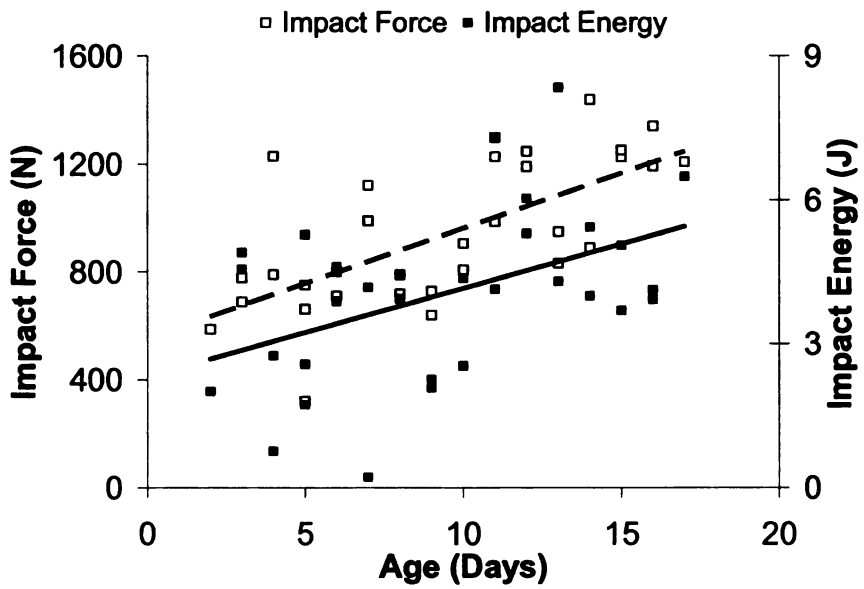

Figure 3.4. Peak impact force with respect to age.

Total fracture length (bone and diastatic) was found to significantly decrease with age at a rate of -1.83 mm/day ($p<0.001$) (Figure 3.5). In 5 of the 31 specimens, no skull fracture (bone or diastatic) was documented.

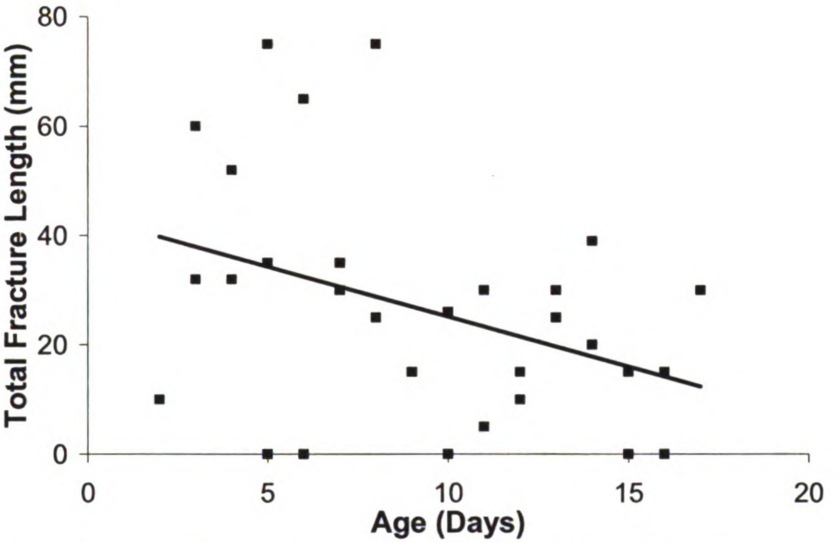

Figure 3.5. Total fracture length with respect to age for free fall and entrapped impacts.

Average diastatic and bone fracture were compared at each age (Figure 3.6). Diastatic fracture was documented as early as 3 days of age. However, no diastatic fracture was noted in specimens older than 14 days of age.

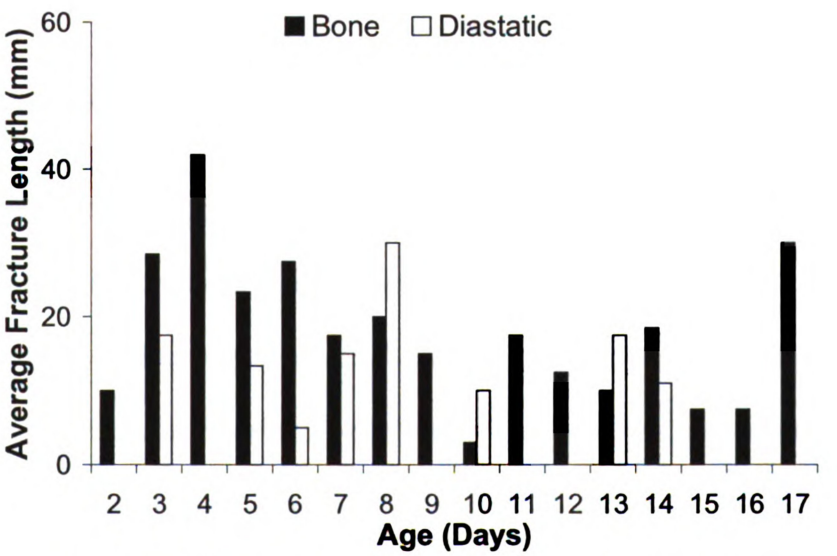

Figure 3.6. The average total fracture length versus age.

In the younger age group (2-9 days old), extensive diastatic fracture was documented along the coronal suture in the free fall impacts (Figure 3.7a). Additionally, several bilateral (occurring on both sides of the suture) bone fractures extended across the coronal suture into the frontal and parietal bones. Bone fracture tended to initiate at the coronal suture. There were no documented initiation sites along the posterior or superior edges of the parietal bone. Also, there was no documented occipital fracture in the free fall head impacts contrasting the extensive occipital fracture noted in Chapter 2 (Figure 3.7b).

Figure 3.7. GIS map of the 2-9 day old age group for the free fall (a) and entrapped (b) impacts.

In the older age group (10-17 days old), several fracture initiations were documented at the lamdoidal and squamosal suture intersection (Figure 3.8a). However, fracture initiation was documented more frequently along the anterior parietal bone as in the younger age group. In Chapter 2, the sites of fracture initiation were frequent and numerous along the perimeter of the parietal bones (Figure 3.8b).

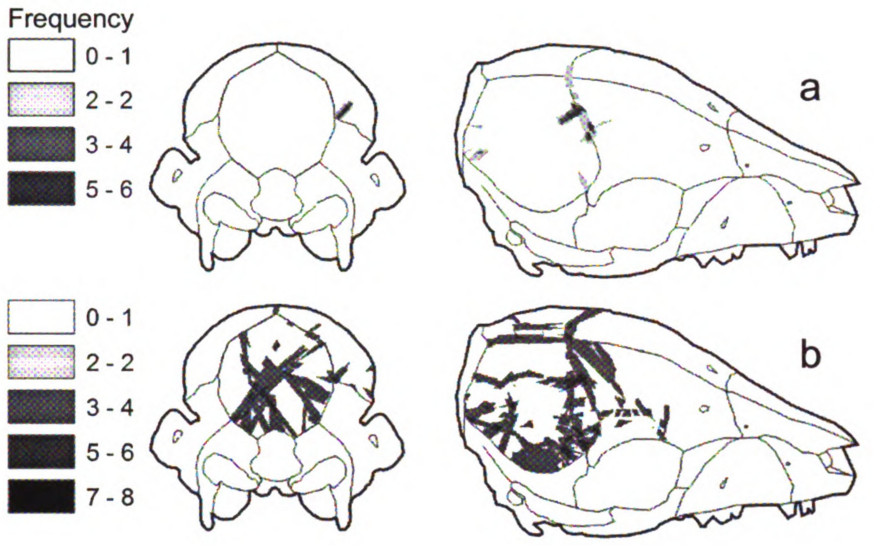

Figure 3.8. GIS map of the 10-17 day old age group for the free fall (a) and entrapped (b) impacts.

As with the young age group, no occipital fracture was documented in the 10-17 day old age group when dropped in free fall. This again contrasted with the extensive occipital fracturing documented for the entrapped head impacts of Chapter 2. Diastatic fracture in the coronal suture was again recorded in the older age group. However, the degree of diastatic fracture was significantly less in the older age group than in the younger.

Several of the older specimens had fracture initiation on either side of the parietal bone at locations remote from the point of impact (Figure 3.9). This was also documented in Chapter 2 and in a previous study using entrapped porcine head rigid impacts (Baumer et al., in press).

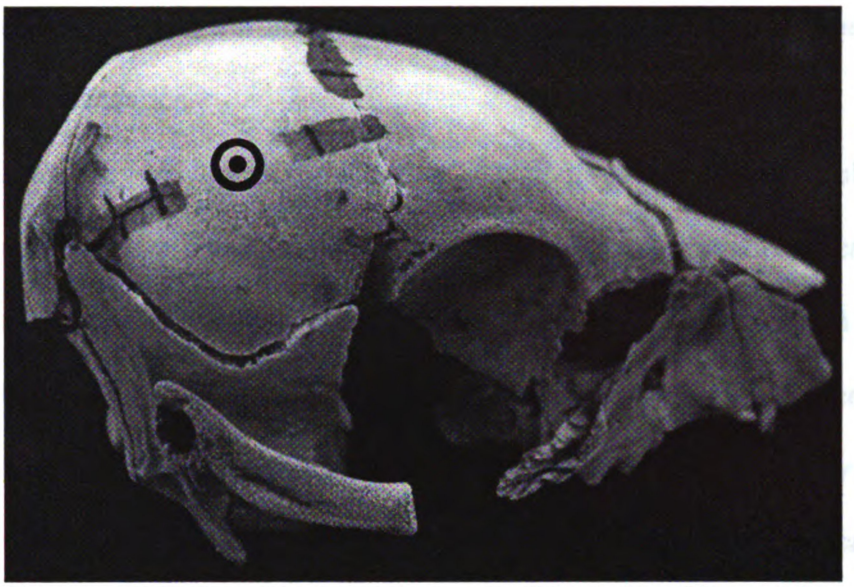

Figure 3.9. Fracture initiation sites located remote of the point of impact (represented by the bull's-eye). Shaded areas represent fractures and each mark represents 5 mm of fracture length.

DISCUSSION

The GIS maps generated in the current chapter did not validate the hypothesis that the pattern of skull fracture was similar between free fall and entrapped head impacts. In Chapter 2, significant occipital fracture was documented in both age groups (2-9 days old and 10-17 days old) for entrapped head impacts at the high level of impact energy. However, in the current chapter the fracturing generated from a free fall head drop, with an equivalent level of impact energy, was confined to the parietal and frontal bones. Thus, it might be hypothesized that the presence of occipital fracture is attributable to an increased state of overall skull stress when the skull is rigidly constrained in the entrapped impacts. Further investigation into this claim will be conducted in Chapter 4. Additionally, diastatic fracture was localized to only the coronal suture for all ages in the free fall impacts. In the entrapped impacts, diastatic was documented extensively in all sutures surrounding the parietal bone for young ages. For older aged specimens, diastatic fracture was documented only in the coronal and sagittal

sutures. These differences further validate that the pattern of fracture changed with different impact scenarios.

In the 2-9 day old age group, the fracture patterns generated from a blunt impact to the entrapped head produced frequent and diffuse fracture initiation sites along the parietal bone boundaries. In the free falls, however, the fracture initiation sites were localized along the coronal suture. However, the two sets of fracture patterns may be used in tandem to diagnose if the head was constrained during the impact by comparing the amount of fracture initiation sites of the victim to the data. The entrapped head fracture patterns provide a better indicator of skull fracture pattern generated from an impact where the head may be resting against a rigid surface. An example of this may be when a victim's head is pinned against a concrete wall and is struck with a blunt weapon such as a club. The fracture patterns generated from the free fall head impacts would be more representative of cases where the victim fell from a highchair or countertop or from a trip and fall incident during the development of walking motor skills. If in a case of potential child abuse, the victim has few initiation sites located along the coronal suture, from the current study data, it can be reasoned that the trauma was due to some sort of free falling head impact with a rigid surface. While abuse cannot be ruled out (the child may have been pushed over), it does rule out a blow to the head while the child's head was constrained with an equal impact energy.

In the current study, the pig model was dropped onto the right parietal bone for better comparison to the data in Chapter 2, which also involved impact trauma to the right parietal bone. The two studies were conducted to record differences in fracture patterns between the two impact scenarios. The literature has shown that the most

commonly fractured cranial bone in both accidental and abuse cases is the parietal (Hobbs, 1984; Meservy et al., 1987; Leventhal et al., 1993) and thus it was reasonable that the targeted impact area of the skull in Chapter 2 and 3 should be the parietal. However, it has been documented in the literature that accidental falls in children typically result in vertex impacts to the head (Yoganandan and Pintar, 2004). This is attributed to the larger head to body mass ratio of children than adults (Snyder, 1977). It must be noted, however, that not all accidental head injuries occur in this fashion. In a study of 18 children with cranial trauma (Plunkett, 2001), several children fell onto the occipital region and also onto the parietal region in innocent playground accidents. In order for the medical examiner to validate the testimony of the caregiver, the pattern of skull fracture must be known for all impact conditions, including impact locations. In this regard, the current study was limited to parietal bone impacts.

In the free fall impacts, fracturing was typically linear and remote from the point of impact. The fractures in the young specimens were generally bilateral, spanning into both the frontal and parietal bones. However, in the older age group, the fractures were unilateral and present in only the parietal bone. Hobbs (1984) documents that accidental injury typically generated narrow, linear fractures in the parietal bone. The data in this chapter supports this claim but it is unclear why there are bilateral fractures and unilateral fracture differences between the young aged and the older aged specimens. It was suggested in Chapter 2 that higher rates of loading cause young suture tissue to behave more "brittle-like", allowing higher stress distributions into surrounding bones of the skull. This same suggestion can be made for the young aged freely dropped specimens in the current chapter. The impact stresses were distributed into the frontal

bone causing fracture because of the suture's ability to transmit stress at higher rates of loading. In the older aged specimens, the sutures have become more stiff and the skull behaves as a single, complete structure rather than separate entities of bone. This allows the impact stresses to be transmitted over the entire area of the skull reducing the potential of fracture.

The results of this chapter document that a porcine model dropped in free fall produced a different pattern of fracture, for a given energy, than an entrapped head impacted with a blunt object. Interestingly, there was a lack of occipital bone fracture in the free fall cases, which was attributed in Chapter 2 to high levels of impact energy. It was also found that the site of fracture initiation was age-dependent with older specimens having fracture initiation on opposite sides of the parietal bone. Accidental falls are a common occurrence in child development and it is necessary to know the pattern of fracture generated from a free fall head impact. The information produced in this research could prove extremely valuable to forensic pathologists and medical examiners in distinguishing the cause of skull fracture in a potential child abuse case when the circumstances of injury are questionable or unknown.

REFERENCES

Baumer TG, Passalacqua NV, Powell BJ, Newberry WN, Fenton TW, Haut RC, in Press, "Age-Dependent Fracture Characteristics of Rigid and Compliant Surface Impacts on the Infant Skull – A Porcine Model," Journal of Forensic Science.

Baumer TG, Powell BJ, Fenton TW, Haut RC, 2009, "Age Dependent Mechanical Properties of the Infant Porcine Parietal Bone and a Correlation to the Human," Journal of Biomechanical Engineering, **131(11)**, pp. 1-6.

Bertocci G and Pierce MC, 2006, "Applications of Biomechanics Aiding in the Diagnosis of Child Abuse," Clinical Pediatric Emergency Medicine, **7(3)**, pp. 194-199.

Billmire ME and Myers PA, 1985, "Serious head injury in infants: accident or abuse?" Pediatrics, **75**, pp. 340-342.

Chason JL, Fernando OU, Hodgson VR, Thomas LM, Gurdjian ES, 1966, "Experimental Brain Concussion: Morphologic Findings and a New Cytologic Hypothesis," The Journal of Trauma, **6(6)**, pp. 767-779.

Cory CZ, Jones MD, James DS, Leadbeatter S, Nokes LDM, 2001, "The potential and limitations of utilizing head impact injury models to assess the likelihood of significant head injury in infants after a fall," Forensic Science International, **123**, pp. 89-106.

Hall JR, Reyes HM, Horvat M, Meller JL, Stein R, 1989, "The Mortality of Childhood Falls," The Journal of Trauma, **29(9)**, pp. 1273-1275.

Hobbs CJ, 1984, "Skull Fracture and the Diagnosis of Abuse", Archives of Disease in Childhood, **59**, pp. 246-252.

Leventhal JM, Thomas SA, Rosenfield NS, Markowitz RI, 1993, "Fractures in young children: distinguishing child abuse from unintentional injuries," American Journal of Diseases of Children, **147**, pp. 87-92.

Marean CW, Abe Y, Nilssen PJ, Stone EC, 2001, "Estimating the Minimum Number of Skeletal Elements (MNE) in Zooarchaeology: A Review and a New Image-Analysis GIS Approach," American Antiquity, **66(2)**, pp. 333-348.

Mayr JM, Seebacher U, Schimpl G, Fiala F, 1999, "Highchair accidents," Acta Pædiatrica, **88(3)**, pp. 319-322.

Meservy CJ, Towbin R, McLaurin RL, Myers PA, Ball W, 1987, "Radiographic characteristics of skull fractures resulting from child abuse," American Journal of Roentgenology, **149**, pp. 173-175.

Plunkett J, 2001, "Fatal Pediatric Head Injuries Caused by Short-Distance Falls," The American Journal of Forensic Medicine and Pathology, **22(1)**, pp. 1-12.

Reece RM and Sege R, 2000, "Childhood Head Injuries: Accidental or Inflicted?" Archives of Pediatric and Adolescent Medicine, **154**, pp. 11-15.

Rosman NP, 2004, "Oski's Essential Pediatrics," In: M Crocetti and MA Barone, editors. Oski's Essential Pediatrics. Philadelphia: Lippincott, Williams, and Wilkins.

Smith MD, Burrington JD, Woolf AD, 1975, "Injuries in children in free falls: an analysis of 66 cases," Journal of Trauma, **15**, pp. 987-991.

Snyder RG, Foust DR, Bowman BM, 1977, "Study of impact tolerance through free fall investigations," IIHS, Washington D.C.

Tabatabaei SM and Sedighi A, 2008, "Pediatric Head Injury," Iranian Journal of Child Neurology, **2(2)**, pp. 7-13.

Wheeler DS and Shope TR, 1997, "Depressed skull fracture in a 7-month old who fell from bed," Pediatrics, **100**, pp. 1033-1034.

Yoganandan N and Pintar FA, 2004, "Biomechanics of temporo-parietal skull fracture," Clinical Biomechanics, **19**, pp. 225-239.

Zimmerman RA and Bilaniuk LT, 1994, "Pediatric head trauma," Neuroimaging Clinics of North America, **4(2)**, pp. 349-366.

CHAPTER FOUR

COMPARISON OF FREE FALL AND ENTRAPPED IMPACTS WITH FINITE ELEMENT ANALYSIS

ABSTRACT

Significant differences exist in the pattern and degree of fracture in head impacts onto a rigid surface and impacts to a constrained head with a rigid interface. In this chapter, fracture length, peak impact force, and impact duration data from the previous two chapters were compared to assess the differences between the two scenarios. Also, finite element simulations were performed using a simplified skull geometry in order to further investigate the differences from a theoretical viewpoint. Peak impact forces were found to be similar regardless of the impact scenario. However, significantly more fracture length was documented in the entrapped porcine head impacts than in the freely dropped heads. Impact durations were significantly longer in the entrapped impacts leading to the assumption that a longer impact duration was the likely explanation for more propagated fractures. Several sources in the literature confirm that a longer duration impact increases the susceptibility of material fracture. The maximum principal tensile stresses were compared between the two impact scenarios using the finite element model. The results showed that the stresses in the entrapped scenario were distributed over a larger area of the skull and were greater in magnitude at locations remote from the point of impact. The free fall simulation produced maximum principal tensile stresses at or nearer to the point of impact. Overlays of the principal stresses onto an experimentally impacted entrapped porcine head showed a strong correlation of fracture pattern between the theoretical finite element model and the experimental data.

However, the free fall principal stresses contrasted the experimental fracture pattern in which fracture initiated at the bone-suture boundary and not at the point of impact which the finite element results suggested. The model was limited, however, to a homogeneous material and simple geometry. A more complex geometry with bone-suture interfaces may provide a better insight into the fracture patterns in the freely dropped porcine heads.

INTRODUCTION

In the previous chapters, two different impact scenarios of the infant porcine skull were tested. In Chapter 2, an entrapped porcine head was impacted with a blunt, rigid mass. These impacts were conducted with a high level of impact energy and generated extensive propagated fractures in the parietal and adjacent bones of the skull. The impact scenario was representative of a constrained head that was impacted with a blunt object, most likely occurring in an inflicted situation. However, a majority of pediatric head trauma is due to accidental falls (Kim et al., 2000; Hall et al., 1989), and thus the porcine head model was tested in free fall in Chapter 3. Significant differences in the fracture patterns were documented in the two studies. Since the level of impact energy in the two studies was the same, the variation in fracture patterns must have been attributed to head constraint.

Often in biomechanics studies, Finite Element Analysis (FEA) is used to determine material stresses and strains in complex geometries or dynamic situations. Several studies have shown that finite element models can be used to correlate clinically or experimentally observed fracture patterns with the stress or strain distributions found from finite element simulations (Silva et al., 1998; Doorly and Gilchrist, 2006; Baumer, 2009; Baumer et al., in press). Modeling fracture of a material typically requires a large computing power, but Frank and Lawn (1967) proposed a theory that principal stress directions could be used to predict the path of fracture propagation. They propose that fracture, as a means of dissipating the maximum amount of energy in a system, occurs perpendicular to the maximum principal stress direction. Therefore, it may be possible to

predict areas of a model that are more susceptible to fracture by investigating the principal stress directions.

In this chapter, a comparison was made between the entrapped head and free fall impact data from the previous two chapters. Fracture length, impact duration, and peak impact force data were revisited from Chapters 2 and 3. Also, finite element analysis was used to simulate the two impact scenarios using a simplified skull geometry. It is thought that by assessing the principal stress magnitude and directions found in the finite element analysis, the change in fracture pattern between entrapped and freely dropped heads could be explained.

MATERIALS AND METHODS

In partnership with Wayne State University, a simplified skull geometry was meshed using the Hexmesher function in DEP Hexmorpher v4.0 (Detroit Engineered Products, Detroit, Michigan) (Figure 1). The diameter of the simplified skull geometry (80 millimeters) was based on the skull size of a 7 day old porcine specimen using CT scans from specimens in Chapter 2. An element size of 0.5 mm was selected, yielding 36,525 solid elements. The outer faces of the hexahedral solids were duplicated to create an overlying skull shell layer with nodal connectivity.

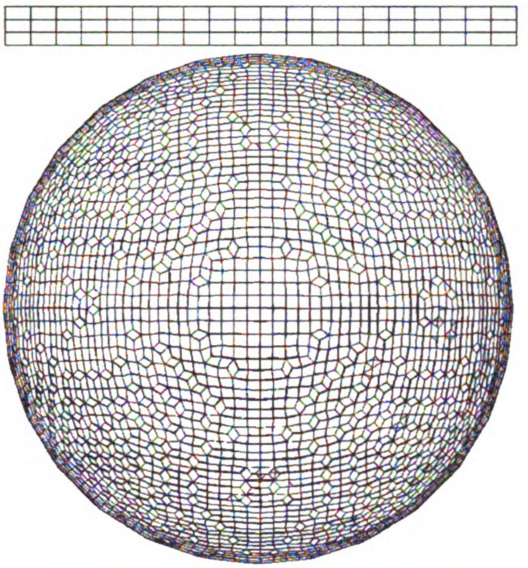

Figure 4.1. Simplified skull geometry used for finite element simulations. Rigid impactor positioned above the skull.

Pre-processing was performed in Altair Hypermesh v9.0 (Altair Engineering, Inc., Troy, Michigan). The solid elements were assigned viscoelastic properties representative of brain tissue (ρ=1,040 kg/m^3, K=211 MPa, G_0=1.72 kPa, G_1=0.51 kPa, decay constant = 20 ms) (Mao et al., 2006). The bulk modulus has limited effect on model predictions, but reducing it by a factor of 10 (from 2.1 GPa) saves computational time (Kleiven, 2002). The brain was added in the model to include intracranial pressure and displacement effects developed by the brain during a blunt impact. This method has been used in previous studies to generate a better predictive model for head impacts (Horgan and Gilchrist, 2004). The skull shell was assigned elastic properties of E=5 GPa (Baumer et al., 2009), ρ=2,150 kg/m^3, and υ=0.28 (Margulies and Thibault, 2000) from the literature. The total head mass was 359 g, which was the average mass of a 2-9 day old pig head (see Appendix B). A skull thickness of 2 mm obtained from the CT scan data was assigned to the shell layer. An 80x80 millimeter rigid impactor with aluminum material properties (ρ=2700 kg/m^3, E=70 GPa, υ=0.35) was positioned 1.4 millimeters

above the sphere to allow initial translation before contact. The rigid impactor had a mass of 1.67 kg, the same mass as the impactor in Chapter 2. Automatic surface-to-surface contact in LS-DYNA (Livemore Software Technology Corporation, Livermore, California) with no penalty stiffness was used to define interaction between the impact interface and sphere. A simulation length of 4 milliseconds was set to show the entire impact duration for both scenarios. The simulations were solved on an Opteron cluster using 1 node (8 CPUs) in LS-DYNA 971r4. Post-processing software (LS PrePost 3.0, Livermore Software Technology Corporation, Livermore, California) was used to assess impact duration, maximum tensile and compressive stress magnitudes, and principal stress directions for each simulation.

Two scenarios were simulated to compare the impact conditions in Chapter 2 and 3. In the first simulation, half of the shell nodes were constrained in the simplified skull to simulate the entrapped head. The constraint condition prevented the simplified skull from translating during the impact. The rigid impactor was assigned an initial velocity of 2.8 m/s to represent a drop height of 40 centimeters. This drop height was used for 3-9 day old entrapped specimens in Chapter 2. In the second simulation, the rigid impactor was constrained to represent an infinite mass. The simplified skull displacement constraints were removed and were given an initial velocity condition of 6.1 m/s to represent a drop height of 1.87 meters. The drop heights were representative of equal impact energies with respect to the mass of the impactor and the head and a static gravitational acceleration (9.81 m/s^2).

Fracture length, impact force, and impact duration data were revisited from Chapters 2 and 3 for comparison. Effects of the impact scenario were assessed for

statistical significance using statistics software (SigmaStat 2.03, Aspire Software International, Ashburn, VA). Two-way ANOVA tests were used to compare the statistical data between the two scenarios. Statistically significant effects were reported for a p-value of less than 0.05.

RESULTS

Total fracture length, impact duration, and peak impact force data from Chapters 2 and 3 were compared. There was significantly more total skull fracture at each age in the entrapped head impacts than in the free fall experiments ($p<0.001$) (Figure 4.2). Comparing the linear regression slopes and intercepts, the slopes were not found to be significantly different ($p=0.2106$), however, the intercepts were statistically different ($p<0.05$).

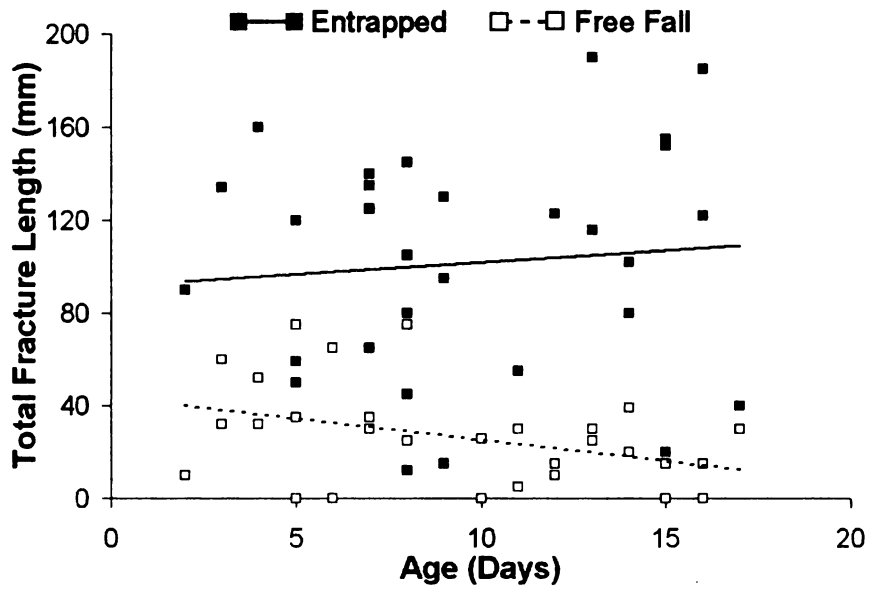

Figure 4.2. Total fracture (diastatic and bone) length with respect to specimen age for both impact scenarios.

A two-way ANOVA analysis showed that the revisited peak impact force data from Chapters 2 and 3 was not statistically different between the free fall and entrapped impacts (Figure 4.3).

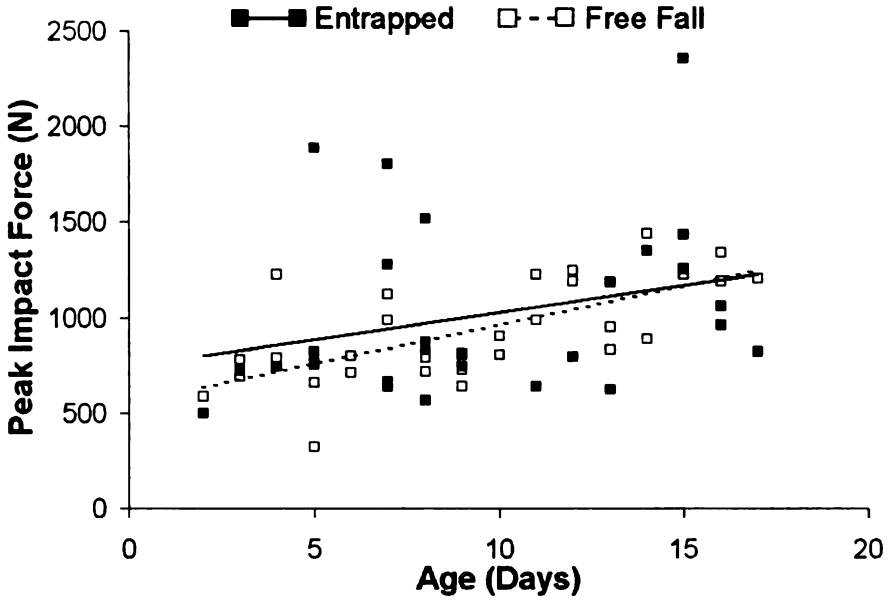

Figure 4.3. Peak impact force with respect to age for both free fall and entrapped impacts.

Impact duration was defined as the total time taken until the peak impact forces began to decrease (Figure 4.4).

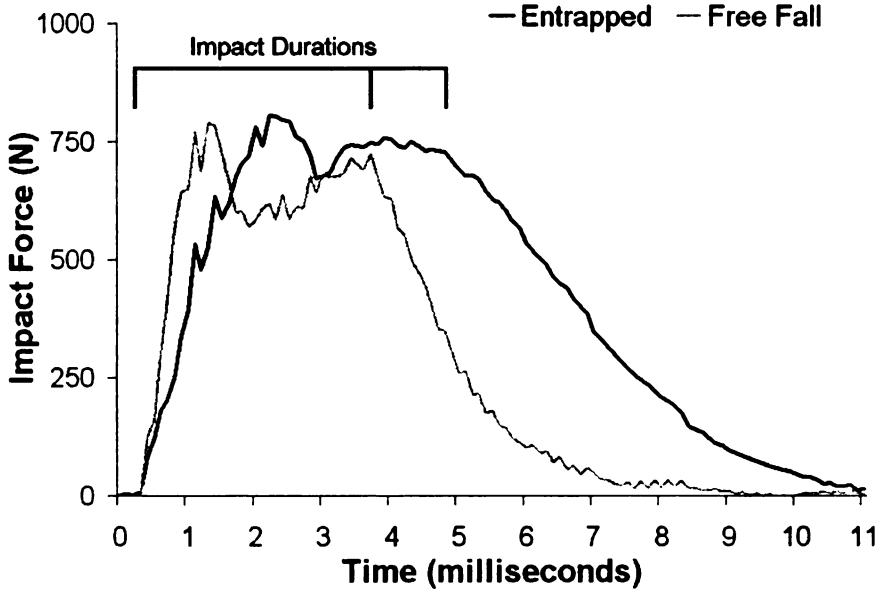

Figure 4.4. Force versus time plots used to determine the duration of impact for both entrapped and free fall impact scenarios.

The impact duration was significantly shorter in the experimental free fall impacts for a given age than the experimental entrapped impacts ($p<0.001$) (Figure 4.5). Linear regression analysis showed shorter impact durations with an increase in age for both scenarios. The theoretical impact durations taken from the finite element simulations were 1.1 ms and 4 ms for the free fall and entrapped impacts, respectively.

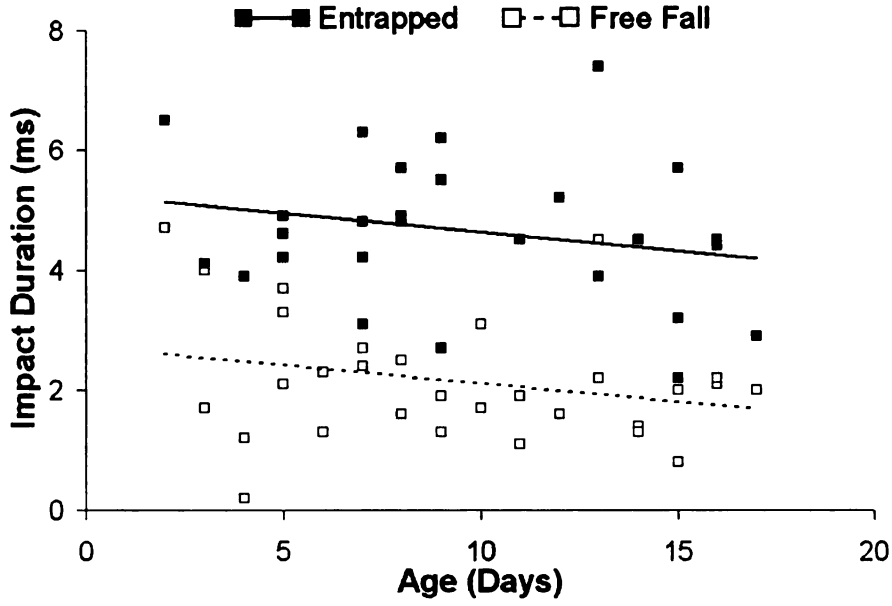

Figure 4.5. Impact duration with respect to age for the free fall and entrapped impacts.

The finite element simulations for the entrapped simplified geometry showed maximum tensile stresses in areas remote of the impact site (Figure 4.6).

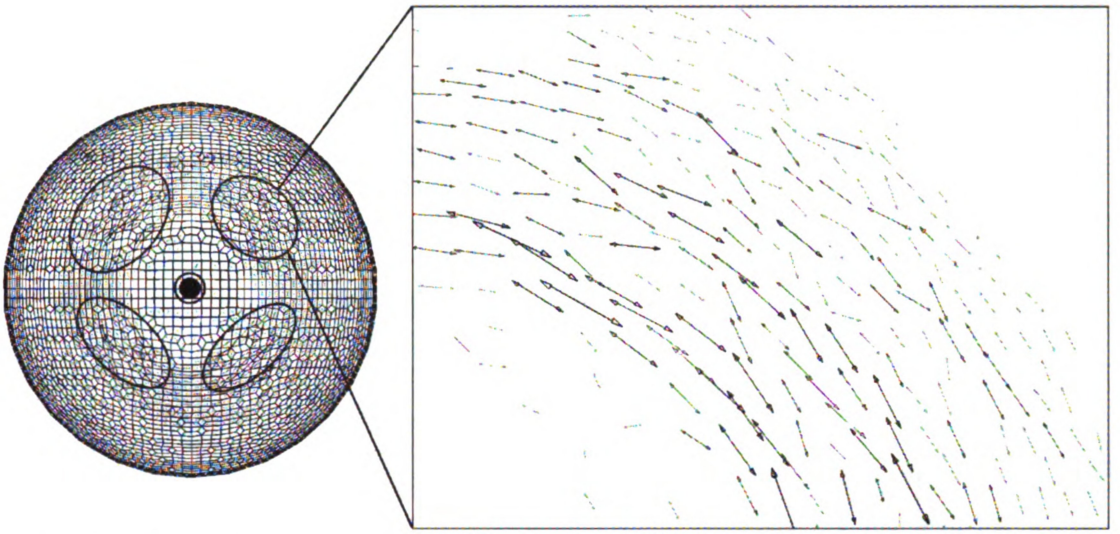

Figure 4.6. Entrapped simulation showing impact site (bull's-eye) and surrounding principal tensile stress directions. Four primary areas of maximum principal tensile stress were documented. Darker arrows represent higher magnitudes of tensile stress.

These principal tensile directions and magnitudes were overlaid on a photo of an entrapped porcine skull to compare the distribution of stresses to the experimental fractures (Figure 4.7).

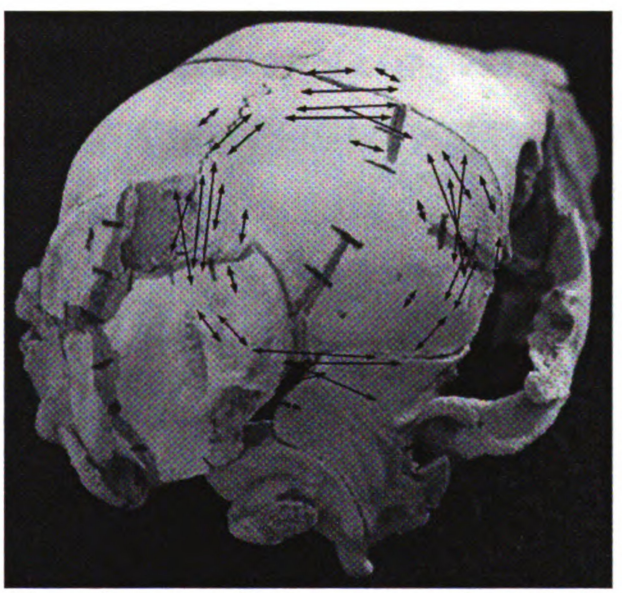

Figure 4.7. Overlaid maximum tensile stress magnitudes and directions on a typical pattern of fractures from an experimental entrapped porcine specimen. Shaded areas indicate documented fracture with each line representing 5 millimeters.

For the free fall simulations, maximum principal stress magnitudes were located nearer the point of impact (Figure 4.8). At points further from the point of impact, the tensile stresses diminished rapidly.

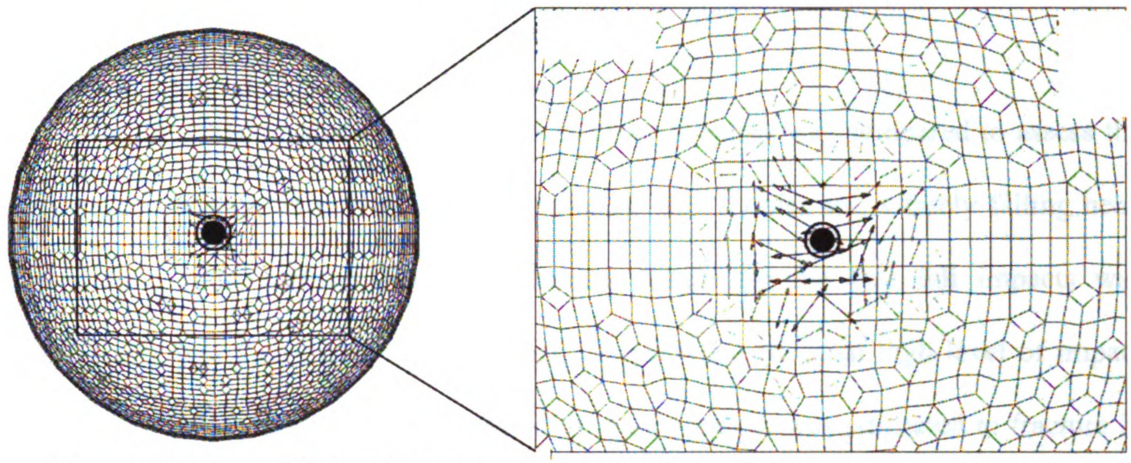

Figure 4.8. Free fall simulation showing impact site (bull's-eye) and surrounding principal tensile stress directions. The largest magnitude of tensile stress was located near the point of impact.

The free fall maximum principal stresses were also overlaid onto an experimentally impacted free fall specimen to compare the observed patterns of fracture with the principal stress magnitudes and directions (Figure 4.9).

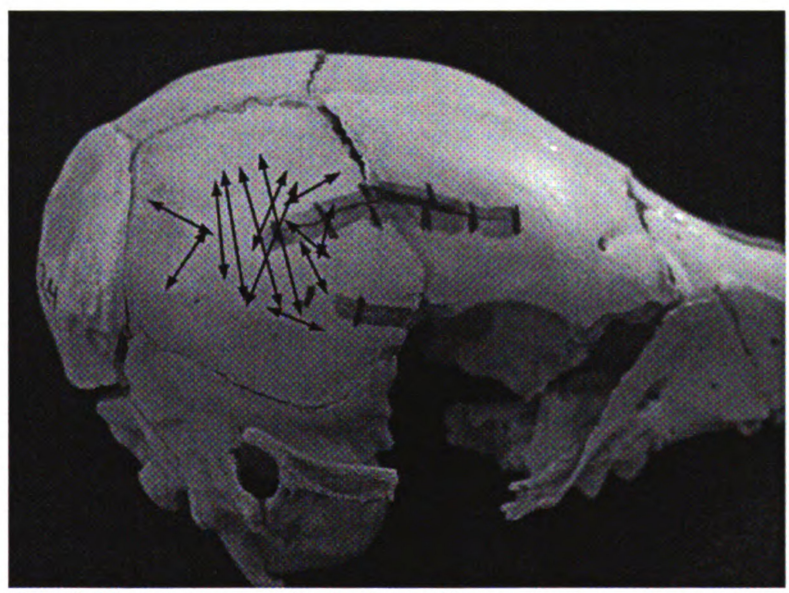

Figure 4.9. Overlaid maximum principal tensile stresses on an experimental free fall porcine skull.

Maximum pressures of the brain were an order of magnitude higher in the entrapped simulation than the free fall pressures (5.41 MPa in the entrapped versus 500 kPa in the free fall).

DISCUSSION

In this chapter, data from the previous two chapters was compared to assess the differences between an entrapped head impacted with a mass and a freely falling head impacting a rigid surface. The total fracture length for the free fall impacts was significantly less than that for the entrapped impacts for an equal high level of impact energy. The larger fracture length in the entrapped scenario was attributed to fracture in the surrounding bones of the skull. In the free fall scenario, the fractures were primarily located in the parietal, although some fracture occurred bilaterally in the frontal bone (Figure 3.7a). Peak impact forces were typically similar for a given age and impact energy, and thus the increased amount of fracture in the entrapped scenarios was not attributed to a higher force of impact. Impact duration, however, was significantly longer in the entrapped specimens than in the free fall. Additionally, the maximum principal stress distributions in the entrapped impacts encompassed a much larger area whereas the free fall stresses were localized around the point of impact.

In the entrapped impacts, a mass was dropped onto a porcine head embedded in epoxy to prevent translation of the head. These impacts were significantly longer in duration than the free fall impacts. In the literature, it has been shown that the density and size of cracks in a brittle solid is affected by the magnitude and duration of an applied dynamic elastic stress field (Evans et al., 1978). Seaman et al. (1976) suggest that propagation of fracture is related to the stress and strain duration. Davis (2000)

documents that the duration and magnitude of the impact forces will determine the extent of cranial injury. Further, Gurdjian (1975) documents that higher and longer intracranial pressure changes can increase the susceptibility of the skull to fracture (Figure 4.10). The intracranial pressures found in the entrapped finite element model support this claim. The entrapped impact scenario produced ten times as much intracranial pressure as the free fall.

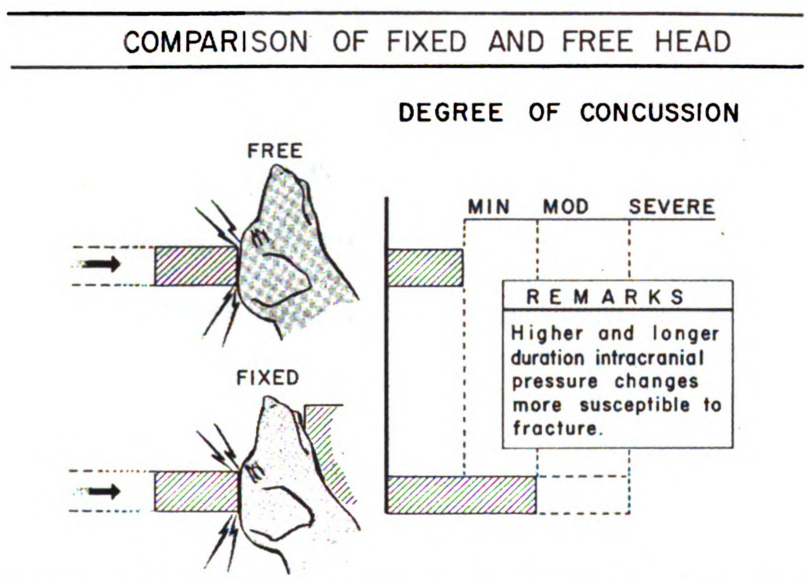

Figure 4.10. Gurdjian's (1975) comparison of the degree of head trauma resulting from a blunt impact to the head. The study suggests that longer duration impacts increase susceptibility of the skull to fracture.

These claims seem reasonable to apply to the current study where there are significant differences in experimental impact duration between two different impact scenarios which generate dramatically different amounts of skull fracture length. The time durations recorded in the theoretical finite element simulations further imply that the process of skull fracture is a time-dependent phenomenon. Mechanically, a longer impact duration places the skull under an elevated stress field for an extended length of time. Assuming the bone fractured at a fraction of the applied stress field, the initiation fracture would continue to propagate under the applied stress field in order to maximize

the energy dissipation. This may explain why there was more propagated fracturing in the entrapped high energy impacts than the free fall impacts where only fracture initiation seemed to have been documented. Further study of fracture models is necessary to verify these claims.

The maximum principal stress magnitudes and directions correlated with the experimentally observed fracture patterns, especially for the entrapped scenario. Frank and Lawn (1967) claim that the greatest amount of energy dissipation occurs when the crack plane is perpendicular to the maximum principal stress direction. They also propose that fracture is the key mechanic in maximizing energy dissipation. In the entrapped scenario, the maximum tensile stresses were documented in areas surrounding the impact site. When overlaid onto a porcine skull, the maximum stresses were not only in the parietal bone but in the occipital bone as well. The principal stress directions were also perpendicular to the key fracture sites. In the free fall simulations, the maximum tensile stresses were located primarily near the point of impact. Using the Frank and Lawn approach, this would suggest that the skull fractures should have been located near the point of impact or in the immediate surrounding area. However, the free fall impacts typically generated small fracture initiation sites away from the point of impact near the sutures surrounding the parietal bone. The mechanism of fracture is therefore somewhat uncertain. The simulation geometry is restricted in that it is a homogeneous bone layer with a brain solid interior. There were no sutures with appropriate material properties to affect the principal stress & strain distributions across the skull (Herring and Teng, 2000). It may be possible that the fracture initiation occurs at the bone-suture boundaries

due to stress and strain concentrations in the bone-suture interface (Baumer et al., in press; Yu et al., 2004; Alexandridis et al., 1985).

In summary, the fracture length, impact duration and peak impact force data from the previous chapters was compared. Fracture length was much greater in the entrapped impacts than the free falls. This was attributed to the entrapped impacts having longer impact durations. Longer impact durations promote fracture propagation in an attempt to maximize the energy dissipation in the system. Also, a finite element software package was used to simulate the two impact scenarios using a simplified skull geometry to validate the increased amount of fracture length documented in the experimental entrapped skull impacts. It was found that an entrapped impact produced a larger distribution of maximum principal tensile stresses across the entire skull, whereas the free fall impacts generated a more localized maximum principal stress pattern near the point of impact. The model, however, was limited in geometry and lacked interfacial changes between the bone and sutures. In order to better understand the mechanisms of remote fractures near the sutures in the experimentally observed free fall scenarios, a more complex model of the immature skull is likely required. Furthermore, the current study suggests that mechanisms of bone and suture damage in the pediatric skull may be very dependent on temporal stress-strain effects. A purely elastic analysis may therefore not be appropriate.

REFERENCES

Alexandridis C, Caputo AA, Thanos CE, 1985, "Distribution of stresses in the human skull," Journal of Oral Rehabilitation, **12(6)**, pp. 499-507.

Baumer TG, 2009, "Material Property Documentation and Fracture Analyses of the Developing Skull," Masters Thesis Dissertation. East Lansing (MI): Michigan State University.

Baumer TG, Nashelsky M, Hurst CV, Passalacqua NV, Fenton TW, Haut RC, in press, "Characteristics and Prediction of Cranial Crush Injuries in Children," Journal of Forensic Science.

Baumer TG, Powell BJ, Fenton TW, Haut RC, 2009, "Age Dependent Mechanical Properties of the Infant Porcine Parietal Bone and a Correlation to the Human," Journal of Biomechanical Engineering, **131(11)**, pp. 1-6.

Davis AE, 2000, "Mechanisms of Traumatic Brain Injury: Biomechanical, Structural and Cellular Considerations," Critical Care Nursing Quarterly, **23(3)**, pp. 1-13.

Doorly MC and Gilchrist MD, 2006, "The use of accident reconstruction for the analysis of traumatic brain injury due to head impacts arising from falls," Computer Methods in Biomechanics and Biomedical Engineering, **9(6)**, pp. 371-377.

Evans AG, Gulden ME, Rosenblatt M, 1978, "Impact damage in brittle materials in the elastic-plastic response régime," Proceedings of the Royal Society of London, **A361**, pp. 343-365.

Frank F and Lawn B, 1967, "On the Theory of Hertzian Fracture," Proceedings of the Royal Society of London, **299(1458)**, pp. 291-306.

Gurdjian ES, 1975, "Impact Head Injury," Charles C. Thomas, Springfield, IL.

Hall JR, Reyes HM, Horvat M, Meller JL, Stein R, 1989, "The Mortality of Childhood Falls," The Journal of Trauma, **29(9)**, pp. 1273-1275.

Herring SW and Teng S, 2000, "Strain in the braincase and its sutures during function," American Journal of Physical Anthropology, **112(4)**, pp. 575-593.

Horgan TJ and Gilchrist MD, 2004, "Influence of FE model variability in predicting brain motion and intracranial pressure changes in head impact simulations," International Journal of Crashworthiness, **9(4)**, pp. 401-418.

Kim KA, Wang MY, Griffith PM, Summers S, Levy ML, 2000, "Analysis of pediatric head injury from falls," Neurosurgical Focus, **8**, Article 3.

Kleiven S, 2002, "Finite Element Modeling of the Human Head," Doctoral Thesis Dissertation. Stockholm, Sweden: Royal Institute of Technology.

Mao H, Zhang L, Yang K, King A, 2006, "Application of a finite element model of the brain to study traumatic brain injury mechanisms in the rat," Stapp Car Crash Journal, **50**, pp.583-600.

Margulies S and Thibault K, 2000, "Infant Skull and Suture Properties: Measurements and Implications for Mechanisms of Pediatric Brain Injury," Journal of Biomechanical Engineering, **122(4)**, pp. 364-371.

Seaman L, Curran DR, Shockey DA, 1976, "Computational models for ductile and brittle fracture," Journal of Applied Physics, **47(11)**, pp. 4814-4826.

Silva MJ, Keaveny TM, Hayes WC, 1998, "Computed Tomography-Based Finite Element Analysis Predicts Failure Loads and Fracture Patterns for Vertebral Sections," Journal of Orthopaedic Research, **16(3)**, pp. 300-8.

Yu JC, Borke JL, Zhang G, 2004, "Brief synopsis of cranial sutures: Optimization by adaptation," Seminars in Pediatric Neurology, **11(4)**, pp. 249-255.

CHAPTER FIVE

CONCLUSIONS AND RECOMMENDATIONS FOR FUTURE WORK

This thesis documented the fracture characteristics of the infant porcine skull as a function of specimen age, impact interface, level of impact energy, and impact scenario. The fracture patterns resulting from a high energy blunt impact to the parietal bone were documented using GIS software. Porcine heads were dropped from a controlled height onto a rigid interface to assess the differences in the pattern of skull fracture between two impact scenarios: free fall and entrapped head impacts. Finally, a simplified skull geometry was modeled in a finite element software package to investigate potential explanations for differences in the fracture lengths and distributions of fracture documented in the entrapped and free fall head experiments.

In Chapter 2, high energy blunt impacts of infant porcine skulls were conducted in order to study characteristic patterns of propagated skull fracture. It was found that new fracture initiation sites were generated in these higher energy impacts that were dependent on impact interface. A rigid interface produced numerous new fracture initiation sites, while the compliant interface produced only one. Additionally, the rigid interface produced more skull fracture than the compliant at all ages except for 2 days for an equal amount of impact energy. GIS was used to document the frequency of characteristic fractures sites generated for both interfaces and at high and low (revisited data from Baumer et al, in press) impact energy levels. Several unique characteristic fractures were documented for each interface, age and energy level impact. One example of these characteristic fractures was a rigid mass striking a constrained head with a high level of impact energy produced a pattern of skull fracture including parietal, occipital

and diastatic fractures. This combination and location of fracturing was unique to only the high energy, rigid impacted specimens and was thus a characteristic fracture pattern for those impact conditions. If given a similar pattern in a case of potential child abuse, it may help in diagnosing whether the trauma was accidental or inflicted. Further studies should focus on continued development of these characteristic fractures using different ages, interfaces and impact energy levels. A comparative database describing fracture characteristics based on the input conditions may be used to eliminate or validate causes of trauma in cases of potential abuse.

In Chapter 3, porcine heads were dropped onto a rigid mass using a gravity accelerated drop trolley. It was found that the pattern of fracture was different than that of the entrapped head impacts for an equal level of impact energy. Fractures in the free fall head drops were typically located in the parietal bone, however in younger aged specimens the fractures extended bilaterally into the frontal bone, producing fracture on either side of the coronal suture (Figure 3.7a). The suture is thought to transmit the impact stresses to surrounding bones by its inherent stiffening during high rates of loading which may help explain the bilateral fractures shown in the younger specimens. In the older age group, the sutures are more developed and the impact stresses are likely distributed more uniformly across the entire skull, reducing the potential for skull fracture. Extensive damage at the coronal suture was documented regardless of age so it is reasonable that a large portion of the impact stresses were located near or were transmitted through the coronal suture. Occipital fracture was not documented in the free fall impacts which significantly contrasted the high energy entrapped impact fracture patterns. These results suggest that the anterior parietal bone and coronal suture

boundary is the weakest section of the skull in these impacts (Macdonald et al., 1988; Burstein and Frankel, 1971). Ultimately, the differences in fracture patterns documented in this chapter could help in future diagnoses of whether a victim's head was constrained during impact. Future work should investigate the differences in skull fracture patterns due to different impact interfaces, impact energies, and impact locations using the free fall porcine head model. A different impact energy or impact interface may produce a different pattern of skull fracture than documented in this study for a high energy, rigid, free fall impact. A larger range of fracture patterns may produce characteristic features of skull fracture depending on each set of input conditions. These characteristic features may prove to be extremely valuable for forensic pathologists and medical examiners to compare to potential child abuse cases to better diagnose the causation of trauma.

In Chapter 4, a simplified skull geometry was modeled using a finite software package. Two simulations were conducted to assess the differences in maximum principal tensile magnitude and directions between the impact scenarios presented in Chapters 2 and 3. Total fracture length, peak impact force, and impact duration data from Chapters 2 and 3 were also compared. Total fracture length was found to be significantly greater in the entrapped impacts than in the free fall. However, there was little difference in peak impact force for a given age, and thus the increased fracturing was not attributed to impact force. The impact duration was significantly greater in the entrapped scenarios then the free falls for a given age. The literature suggests that a longer impact duration under a dynamic stress field makes the skull more susceptible to fracture. Also, the maximum principal stresses were distributed over a larger area of the entrapped simplified skull in the finite element simulations than the freely falling skull.

Using an overlay of these principal stress magnitudes and directions, it was noted that the experimental skull fractures compared well with the theoretical stress directions for the entrapped scenario, however the free fall experimental fractures did not resemble the theoretical predictions. Further studies should use a more complex and realistic skull geometry taken from a computed-tomography (CT) scan to investigate principal stress differences due to the more complex geometry. The model should also include sutures to assess how the impact stresses are affected by a non-homogeneous material and interface conditions between the bone and suture. It has been shown that increased levels of strain exist at the sutures during impact which may be a key indicator of why fracture initiation occurs at the bone-suture boundary in the free fall impacts (Baumer, 2009).

This research was based on assessing the degree and pattern of fracture of an infant porcine head model impacted in two injury scenarios. It was found that specimen age as well as impact interface, energy, and scenario all contribute to the pattern and degree of skull fracture in a porcine head model. This work suggests that investigating characteristic patterns of fracture may aid in producing a more robust predictive fracture model to help diagnose accidental trauma from inflicted. Pattern recognition techniques currently used for fingerprints could potentially help quantify these characteristic fracture patterns for each set of impact conditions. With a database of characteristic fracture patterns for a wide range of impact conditions, a forensic pathologist or medical examiner may be able to find a causation of trauma based on a victim's skull fracture pattern.

REFERENCES

Baumer TG, 2009, "Material Property Documentation and Fracture Analyses of the Developing Skull," Masters Thesis Dissertation. East Lansing (MI): Michigan State University.

Baumer TG, Passalacqua NV, Powell BJ, Newberry WN, Fenton TW, Haut RC, in press, "Age-Dependent Fracture Characteristics of Rigid and Compliant Surface Impacts on the Infant Skull – A Porcine Model," Journal of Forensic Science.

Burstein AH and Frankel VH, 1971, "A standard test for laboratory animal bone," Journal of Biomechanics, **4(2)**, pp. 155-158.

Macdonald W, Skirving AP, Scull ER, 1988, "A device for producing experimental fractures," Acta orthopaedica Scandinavica, **59(5)**, pp. 542-544.

APPENDIX A
RAW DATA FROM CHAPTER 2

Table A.1. Raw data from high energy rigid interface impacts.

Specimen	Age (days)	Drop Height (cm)	Falling Mass (g)	Impact Force (N)	Displacement at Max Load (mm)	Impact Duration (s)	Failure Energy (J)	Stiffness (kN/m)
PI058	2	20	1564	499.27	8.37	0.0065	2.232	110.02
PI109	3	40	1669	724.21	10.00	0.0041	3.171	92.65
PIHE018	4	40	1669	741.17	10.28	0.0039	4.146	218.22
PI125	5	40	1669	764.25	9.60	0.0042	3.755	144.99
PI129	5	40	1669	822.35	10.77	0.0046	4.491	134.49
PIHE017	5	40	1669	1885.79	11.49	0.0049	5.558	195.77
PI113	7	40	1669	639.23	10.27	0.0042	3.204	151.04
PIHE006	7	40	1669	1276.69	14.06	0.0063	5.779	222.61
PIHE008	7	40	1669	1804.61	12.34	0.0048	4.892	261.75
PIHE009	7	40	1669	663.12	8.16	0.0031	2.509	401.326
PIHE001	8	40	1919	Computer malfunction, data not recorded - impact still reported due to skull damage				
PIHE002	8	40	1669	833.08	10.95	0.0048	4.948	185.61
PIHE005	8	40	1669	875.56	11.39	0.0049	5.202	153.98
PIHE007	8	40	1669	1516.83	13.14	0.0057	5.685	154.84
PI110	8	40	1669	566.74	12.92	0.0057	3.920	79.81
PI126	9	40	1669	811.22	12.43	0.0062	4.732	136.96
PIHE015	9	40	1669	806.60	8.20	0.0027	3.232	194.13
PIHE016	9	40	1669	742.40	12.35	0.0055	5.115	117.78
PI130	11	70	1669	639.50	15.73	0.0045	5.366	122.68
PI116	12	70	1669	796.56	15.36	0.0052	6.958	220.56
PI002	13	60	1919	622.94	12.16	0.0039	4.353	166.79
PI006	13	60	1919	1186.29	17.71	0.0074	8.434	219.32
PIHE003	14	70	1669	Computer malfunction, data not recorded - impact still reported due to skull damage				
PIHE004	14	70	1919	1353.93	14.76	0.0045	9.571	183.86
PIHE011	15	70	1669	1258.37	9.10	0.0022	4.818	268.34
PIHE012	15	70	1669	1433.07	11.20	0.0032	7.540	296.16

Table A.1. Continued

Specimen	Age (days)	Drop Height (cm)	Falling Mass (g)	Impact Force (N)	Displacement at Max Load (mm)	Impact Duration (s)	Failure Energy (J)	Stiffness (kN/m)
PIHE013	15	70	1669	2354.25	17.84	0.0057	9.812	311.16
PI111	16	70	1669	963.80	12.98	0.0044	6.956	138.11
PIHE010	16	70	1669	1060.04	14.22	0.0045	7.951	152.64
PI055	17	60	1919	822.35	9.19	0.0029	4.220	290.54
PI070	19	60	1919	833.89	11.54	0.0040	5.924	172.24
PIHE014	19	60	1919	1233.12	13.64	0.0051	9.054	221.75
PIHE022	20	60	1919	Computer malfunction, data not recorded - impact still reported due to skull damage				
PIHE023	20	60	1919	1213.57	13.60	0.0047	9.312	154.25
PIHE026	24	70	1919	1174.07	11.08	0.0034	7.536	355.41
PIHE027	24	70	1919	1306.83	14.56	0.0055	11.411	381.38
PIHE030	28	120	1919	1506.51	164.02	0.0015	5.431	214.52
PIHE031	28	120	1919	2311.08	11.93	0.0018	7.509	534.40

Table A.2. Thickness, fracture length, and contact area measurements for high energy rigid interface impacts.

Specimen	Age (days)	Average Thickness (mm)	Bone Fracture (mm)	Suture Damage (mm)	Total Damage (mm)	Contact Area (mm^2)
PI058	2	1.28	72	18	90	64.2
PI109	3	1.03	118	16	134	264.9
PIHE018	4	1.05	135	25	160	463.1
PI125	5	1.15	39	20	59	41.0
PI129	5	1.18	120	0	120	155.3
PIHE017	5	1.14	50	0	50	326.0
PI113	7	0.99	80	45	125	53.7
PIHE006	7	1.33	140	0	140	443.3
PIHE008	7	1.15	65	0	65	256.2
PIHE009	7	1.12	135	0	135	478.8
PIHE001	8	-	85	20	105	207.3
PIHE002	8	-	73	7	80	146.3
PIHE005	8	1.47	12	0	12	276.6
PIHE007	8	1.43	45	0	45	451.8
PI110	8	1.06	90	55	145	225.6
PI126	9	1.42	15	0	15	103.6
PIHE015	9	1.99	95	0	95	339.0
PIHE016	9	1.27	130	0	130	251.5
PI130	11	0.95	30	25	55	NO PF
PI116	12	1.64	123	0	123	349.2
PI002	13	1.84	95	21	116	158.6
PI006	13	1.02	190	0	190	120.4
PIHE003	14	-	80	22	102	224.0
PIHE004	14	1.73	80	0	80	155.3
PIHE011	15	2.00	155	0	155	622.9
PIHE012	15	1.93	20	0	20	492.0
PIHE013	15	1.08	115	37	152	235.6
PI111	16	2.01	95	27	122	278.8
PIHE010	16	2.28	185	0	185	549.1
PI055	17	1.53	40	0	40	248.6
PI070	19	1.41	220	0	220	61.9
PIHE014	19	1.78	35	0	35	520.3
PIHE022	20	2.28	105	0	105	580.8
PIHE023	20	2.73	225	15	240	695.2
PIHE026	24	2.91	90	0	90	628.2
PIHE027	24	2.72	165	0	165	706.9
PIHE030	28	2.59	65	0	65	584.9
PIHE031	28	3.92	55	0	55	810.1

Table A.3. Raw data from high energy compliant interface impacts.

Specimen	Age (days)	Drop Height (cm)	Falling Mass (g)	Impact Force (N)	Displacement at Max Load (mm)	Impact Duration (s)	Failure Energy (J)	Stiffness (kN/m)
PIHE019	3	40	1669	758.96	10.53	0.0040	4.162	195.69
PIHE040	4	40	1669	779.86	14.47	0.0078	6.120	106.98
PIHE020	5	40	1669	589.68	15.88	0.0066	4.966	83.27
PIHE041	5	40	1669	762.08	4.89	0.0017	1.000	171.55
PIHE039	6	40	1669	781.63	15.17	0.0075	5.882	94.13
PIHE042	7	40	1669	678.46	15.11	0.0074	5.772	117.32
PIHE038	8	40	1669	632.31	14.26	0.0069	5.760	84.61
PIHE021	10	60	1669	Computer malfunction, data not recorded - impact still reported due to skull damage				
PIHE043	10	60	1669	1001.26	13.18	0.0043	6.980	89.70
PIHE037	11	70	1669	971.81	15.60	0.0049	8.147	164.52
PIHE036	13	70	1669	1197.15	15.35	0.0049	8.950	144.72
PIHE044	18	60	1919	1125.34	5.38	0.0015	1.186	180.25
PIHE024	20	60	1919	1278.32	13.14	0.0037	6.275	197.59
PIHE025	20	60	1919	1323.39	12.71	0.0045	8.389	225.20
PIHE028	24	70	1919	1446.24	15.63	0.0056	11.327	195.55
PIHE029	24	70	1919	Computer malfunction, data not recorded - impact still reported due to skull damage				
PIHE034	24	70	1919	1339.95	17.38	0.0053	10.558	105.20
PIHE032	28	120	1919	1682.98	15.66	0.0026	9.637	131.43
PIHE033	28	120	1919	1648.37	22.81	0.0050	18.806	118.84

Table A.4. Thickness, fracture length, and contact area measurements for high energy compliant interface impacts.

Specimen	Age (days)	Average Thickness (mm)	Bone Fracture (mm)	Suture Damage (mm)	Total Damage (mm)	Contact Area (mm^2)
PIHE019	3	1.18	90	10	100	756.2
PIHE040	4	1.46	45	20	65	464.5
PIHE020	5	1.08	55	15	70	796.3
PIHE041	5	1.23	95	20	115	842.7
PIHE039	6	1.31	30	25	55	472.9
PIHE042	7	1.02	105	15	120	724.3
PIHE038	8	1.64	45	0	45	621.9
PIHE021	10	1.66	175	0	175	480.3
PIHE043	10	1.58	100	0	100	906.1
PIHE037	11	2.42	5	0	5	844.0
PIHE036	13	2.31	10	0	10	580.5
PIHE044	18	1.38	145	25	170	995.2
PIHE024	20	2.23	100	0	100	824.6
PIHE025	20	2.37	35	0	35	918.9
PIHE028	24	2.18	35	0	35	687.5
PIHE029	24	2.27	115	0	115	807.2
PIHE034	24	2.51	0	0	0	1133.1
PIHE032	28	2.83	70	5	75	1311.6
PIHE033	28	2.62	0	0	0	1394.9

APPENDIX B
RAW DATA FROM CHAPTER 3

Table B.1. Raw data collected from free fall rigid interface impacts.

Specimen	Age (days)	Drop Height (cm)	Head Mass (g)	Impact Force (N)	Displacement at Max Load (mm)	Impact Duration (s)	Failure Energy (J)	Stiffness (kN/m)
003FF02	2	89.4	350	586.83	8.78	0.0047	2.007	139.44
021FF03	3	174.4	380	777.28	48.02	0.0040	4.905	115.40
022FF03	3	174.4	380	688.91	60.63	0.0017	4.557	199.35
024FF04	4	176.7	375	1228.23	11.83	0.0002	0.759	156.99
025FF04	4	176.7	375	789.64	9.06	0.0012	2.749	189.24
001FF05	5	81.3	500	319.75	12.25	0.0033	1.726	24.56
002FF05	5	132.5	500	751.15	13.48	0.0037	5.273	193.05
005FF05	5	132.5	500	661.70	11.63	0.0021	2.572	76.23
017FF06	6	167.7	395	800.29	60.57	0.0013	3.884	182.79
018FF06	6	167.7	395	710.97	29.61	0.0023	4.612	112.53
026FF07	7	189.3	350	1120.59	8.77	0.0027	0.216	119.59
027FF07	7	189.3	350	989.52	14.52	0.0024	4.181	79.04
011FF08	8	154.1	430	718.37	12.73	0.0025	4.423	166.26
012FF08	8	154.1	430	789.98	29.27	0.0016	3.939	164.45
004FF09	9	119.4	555	639.16	10.34	0.0019	2.080	52.08
008FF09	9	119.4	555	728.35	7.62	0.0013	2.256	205.95
006FF10	10	132.5	500	906.11	17.29	0.0031	4.367	73.53
007FF10	10	132.5	500	808.17	10.78	0.0017	2.536	115.77
028FF11	11	193.7	605	1227.49	50.64	0.0019	7.300	184.20
029FF11	11	193.7	605	986.88	45.87	0.0011	4.138	176.50
030FF12	12	184.6	635	1246.69	40.25	0.0016	5.299	151.76
031FF12	12	184.6	635	1190.50	31.95	0.0016	6.035	202.19
009FF13	13	118.4	990	832.13	18.28	0.0045	8.342	130.55
010FF13	13	118.4	990	948.80	11.80	0.0022	4.303	109.50
019FF14	14	162.8	720	1438.50	46.98	0.0014	5.432	304.90
020FF14	14	162.8	720	889.27	48.06	0.0013	3.999	160.21

Table B.1. Continued

Specimen	Age (days)	Drop Height (cm)	Head Mass (g)	Impact Force (N)	Displacement at Max Load (mm)	Impact Duration (s)	Failure Energy (J)	Stiffness (kN/m)
013FF15	15	146.5	800	1226.47	21.29	0.0020	5.052	138.66
014FF15	15	146.5	800	1250.83	41.16	0.0008	3.690	433.98
015FF16	16	134.7	870	1340.56	23.37	0.0021	3.927	133.82
016FF16	16	134.7	870	1192.80	23.67	0.0022	4.124	92.60
023FF17	17	171.1	685	1208.01	51.90	0.0020	6.493	151.13

Table B.2. Fracture length and contact area measurements for free fall high energy rigid interface impacts.

Specimen	Age (days)	Bone Fracture (mm)	Suture Damage (mm)	Total Damage (mm)	Contact Area (mm^2)
003FF02	2	10	0	10	13.828
021FF03	3	40	20	60	44.004
022FF03	3	17	15	32	190.561
024FF04	4	32	0	32	61.469
025FF04	4	52	0	52	47.698
001FF05	5	5	30	35	197.919
002FF05	5	65	10	75	58.892
005FF05	5	0	0	0	61.240
017FF06	6	0	0	0	144.123
018FF06	6	55	10	65	129.408
026FF07	7	20	10	30	30.863
027FF07	7	15	20	35	98.058
011FF08	8	30	45	75	91.559
012FF08	8	10	15	25	167.027
004FF09	9	15	0	15	52.708
008FF09	9	15	0	15	153.543
006FF10	10	6	20	26	66.049
007FF10	10	0	0	0	144.925
028FF11	11	5	0	5	129.064
029FF11	11	30	0	30	188.786
030FF12	12	15	0	15	71.489
031FF12	12	10	0	10	77.874
009FF13	13	5	25	30	183.146
010FF13	13	15	10	25	112.144
019FF14	14	20	0	20	328.214
020FF14	14	17	22	39	260.619
013FF15	15	15	0	15	253.061
014FF15	15	0	0	0	205.134
015FF16	16	0	0	0	238.860
016FF16	16	15	0	15	133.072
023FF17	17	30	0	30	140.602